

Research



Cite this article: Cooke GJ, Marsh DR, Walsh C, Black B, Lamarque J-F. 2022 A revised lower estimate of ozone columns during Earth's oxygenated history. *R. Soc. Open Sci.* **9**: 211165. <https://doi.org/10.1098/rsos.211165>

Received: 9 July 2021

Accepted: 25 November 2021

Subject Category:

Earth and environmental science

Subject Areas:

atmospheric science/atmospheric chemistry

Keywords:

ozone layer, Proterozoic Earth, habitability, Faint Young Sun Paradox, Earth system modelling, atmospheric chemistry

Author for correspondence:

G. J. Cooke

e-mail: pygjc@leeds.ac.uk

A revised lower estimate of ozone columns during Earth's oxygenated history

G. J. Cooke¹, D. R. Marsh^{1,2}, C. Walsh¹, B. Black^{3,4} and J.-F. Lamarque²

¹School of Physics and Astronomy, University of Leeds, Leeds LS2 9JT, UK

²National Center for Atmospheric Research, Boulder, CO 80301, USA

³Department of Earth and Planetary Sciences, Rutgers University, Piscataway, NJ, USA

⁴Department of Earth and Atmospheric Sciences, CUNY City College, New York, NY, USA

GJC, 0000-0001-6067-0979; DRM, 0000-0001-6699-494X; CW, 0000-0001-6078-786X; BB, 0000-0003-4585-6438; J-FL, 0000-0002-4225-5074

The history of molecular oxygen (O₂) in Earth's atmosphere is still debated; however, geological evidence supports at least two major episodes where O₂ increased by an order of magnitude or more: the Great Oxidation Event (GOE) and the Neoproterozoic Oxidation Event. O₂ concentrations have likely fluctuated (between 10⁻³ and 1.5 times the present atmospheric level) since the GOE ~2.4 Gyr ago, resulting in a time-varying ozone (O₃) layer. Using a three-dimensional chemistry-climate model, we simulate changes in O₃ in Earth's atmosphere since the GOE and consider the implications for surface habitability, and glaciation during the Mesoproterozoic. We find lower O₃ columns (reduced by up to 4.68 times for a given O₂ level) compared to previous work; hence, higher fluxes of biologically harmful UV radiation would have reached the surface. Reduced O₃ leads to enhanced tropospheric production of the hydroxyl radical (OH) which then substantially reduces the lifetime of methane (CH₄). We show that a CH₄ supported greenhouse effect during the Mesoproterozoic is highly unlikely. The reduced O₃ columns we simulate have important implications for astrobiological and terrestrial habitability, demonstrating the relevance of three-dimensional chemistry-climate simulations when assessing paleoclimates and the habitability of faraway worlds.

1. Introduction

Ozone (O₃), despite only making up a tiny proportion of Earth's atmosphere by weight, is one of the most important molecules for life on Earth. Without the presence of a substantial stratospheric O₃ layer, the surface would receive higher amounts of harmful ultraviolet (UV) radiation. However, this modern day

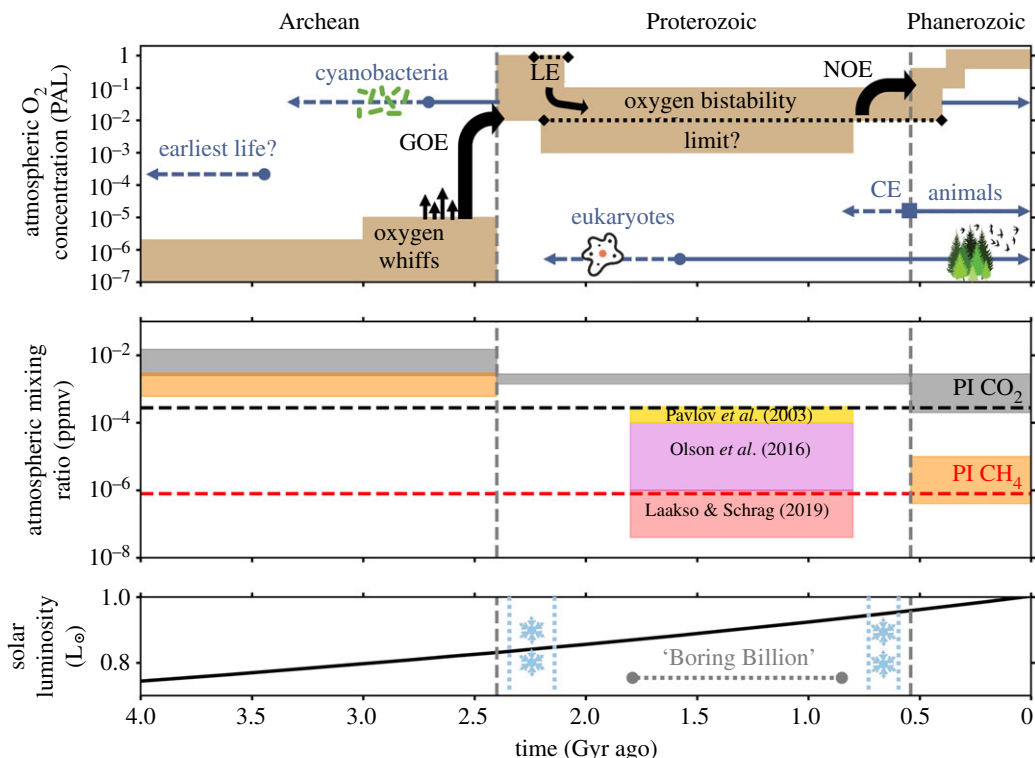


Figure 1. Earth's evolving atmosphere. (*Top*), Geochemical evidence and modelling constraints place approximate limits on the concentration of O₂ during this simplified history of Earth's atmospheric evolution. Brown boxes show the predicted oxygen concentration against time in the past. Grey-blue lines show approximate timelines for the appearance of the earliest life forms [6,7], the evolution of cyanobacteria [8,9], eukaryotes [10–13] and the origin of animals [14,15], with dotted lines showing a period of estimated emergence, and solid lines showing generally accepted presence. Also shown by the grey-blue square symbol is the Cambrian explosion (CE). The upward black curved arrows show approximate dates for major geological episodes of increasing atmospheric oxygenation: the Great Oxidation Event (GOE) and the Neoproterozoic Oxidation Event (NOE). Black dotted lines show the Lomagundi Event (LE) and a proposed oxygen bistability limit at 1% PAL [16]. Indicated by straight black arrows are possible 'whiffs' of increasing oxygenation. Dates and magnitude curves are not exact and there are still many uncertainties associated with several indicated events and O₂ constraints—see Lyons *et al.* [17], Olson *et al.* [18] and Lyons *et al.* [19]. (*Middle*), The estimated ranges for CO₂ and CH₄ are given in terms of parts per million by volume. Conflicting predictions for CH₄ concentrations during the Proterozoic are given by Pavlov *et al.* [20] (yellow), Olson *et al.* [21] (magenta) and Laakso & Schrag [22] (light red). The CH₄ (orange) and CO₂ (grey) ranges in the Phanerozoic and Archean are 'preferred' ranges from Olson *et al.* ([18] and references therein). The red dotted and black dotted lines are the pre-industrial values used in our simulations. (*Bottom*), The estimated luminosity of the Sun is shown with respect to time. The 'Boring Billion' is indicated, as are periods where low-latitude glaciation occurred intermittently [23,24], as shown by the dashed light blue lines next to snowflakes. Solar luminosity data are from Bahcall *et al.* [25].

O₃ layer would not exist without abundant molecular oxygen (O₂), and the Earth's atmosphere has not always been O₂-rich.

Atmospheres in the solar system are continuously changing, and Earth's atmosphere is no exception. From anoxic origins, Earth's atmospheric oxygenation has varied through time, with O₂ now the second most abundant constituent of the atmosphere. The Archean eon (4–2.4 Gyr ago) was, for the most part, a reducing atmosphere, with evidence of temporary periods of increased oxygenation [1–4]. At the end of this period, a rise in oxygen set the scene for an oxygenated biosphere and the eventual evolution of oxygen-dependent animals [5].

Figure 1 gives an overview of the current picture of Earth's oxygenation history. A large rise in oxygen concentrations occurred approximately 2.5–2.4 billion years ago at the start of the Great Oxidation Event (GOE) [19,26]. Mass-independent fractionation of sulphur isotopes in the geological record indicate that O₂ quantities fluctuated for a further approximately 200 Myr [26,27] before an oxygenated atmosphere was permanently established following the GOE [17,23,26,28–30]. Afterwards, oxygen concentrations dropped again [31,32], with oxygen concentrations likely between 10⁻³ and 10⁻¹ the present atmospheric level (PAL equals 21% by volume, the modern day oxygen concentration) for

the rest of the Proterozoic (2.4–0.54 Gyr ago) [17,19]. Some literature estimates suggest a larger range between 10^{-5} and 10^{-1} PAL [5,18,33]. However, recent one-dimensional atmospheric photochemical modelling of Earth's oxygenation history suggests geologically persistent Proterozoic oxygen levels could have been limited to values greater than or equal to 10^{-2} PAL. This is based on predictions of an atmospheric bistability [16,34], where there are two stable (steady-state, converged simulations) regions of high- and trace-oxygen solutions, separated by a region where equilibrium solutions rarely exist. For instance, Gregory *et al.* [16] reported a small proportion (less than 5% of the high and trace- O_2 simulations) of stable solutions to exist between $3 \times 10^{-6}\%$ (0.6 ppmv) and 1% the present atmospheric level of O_2 .

Towards the end of the Proterozoic, there was a further episode of increasing oxygenation known as the Neoproterozoic Oxidation Event [17,35,36], leading into the current Phanerozoic geological eon where oxygen levels have generally been estimated to have varied between 10% PAL and 150% PAL [17,33,37–40] for the past 0.54 billion years, reaching approximate modern-day concentrations during the Paleozoic [19,41,42].

The earliest fossilized animals date back approximately 575 Ma [14,43], roughly 1.7 Gyr after the GOE. Biomarkers imply that demosponges may have emerged before this, perhaps as far back as 660 Ma [44], although this has been disputed [45] and the debate continues [46–48]. Furthermore, analysis of biomolecular clocks (where rates of mutation are analysed to determine the past divergence of species and biological functionalities in lieu of alternative evidence, such as fossils) indicates possible animal life 200 Myr prior to the emergence of animal fossils [15,49]. It has been suggested that Phanerozoic-like oxygen levels were required for complex animal life (metazoans) to diversify [50–52], but not necessarily needed for metazoans to evolve [53], because the emergence of animals may not have coincided with a rise in O_2 [54,55]. Thus, how changing oxygen levels have influenced the evolution of life through time is uncertain [5,53,55] because of early-evolving animals such as sponges that can survive at very low O_2 concentrations [54].

In summary, dramatic changes in atmospheric O_2 levels took place during the period between approximately 2.4 and 0.4 Gyr ago, with uncertainties still covering a large O_2 range [19]. Previous one-dimensional modelling has found that these changes in O_2 strongly impact atmospheric O_3 levels [56–58]. In the modern atmosphere, the O_3 layer protects animal and plant life from harmful UV radiation, but the O_3 layer has not always been present. Rising oxygen levels above 10^{-4} PAL likely formed and increased the UV-protective O_3 column [e.g. see 57,58], where the column is the total number of molecules above the surface per unit area. Fluctuations in the O_3 column have likely affected the evolution of animal and plant life. For example, relatively rapid past reductions in the O_3 layer could have resulted in increased fluxes of biologically harmful UV-B radiation (280–315 nm) at the surface, possibly causing more than one mass extinction event during the Phanerozoic [59–61]. On the other hand, because Phanerozoic-like oxygen concentrations could have been present for approximately 200 Myr during the GOE [17], the protective O_3 column's effect on animal life's origins have been argued to be temporally irrelevant [55,62].

It is not just O_2 and O_3 concentrations that have changed since the dawn of Earth's atmosphere. The Sun's luminosity has been steadily increasing through time—see figure 1. The increased luminosity is due to the Sun fusing hydrogen into helium, which causes the central temperature and density of the Sun to increase [25], quickening the rate of fusion. The Sun's luminosity is estimated to have been 74% and 86% of today's solar luminosity, 4 Gyr ago and 2 Gyr ago, respectively [25].

The Mesoproterozoic (1.8–0.8 Gyr ago), often referred to as the 'Boring Billion', was reportedly free of widespread glaciation [24,63]. This is paradoxical, because a fainter Sun during this period would result in increased ice coverage, all other atmospheric properties being equal. This problem is the 'Proterozoic Faint Young Sun Paradox'. To mitigate the fainter Sun during various geological periods, prior research has suggested that an increased greenhouse effect is required [64–67]. Specifically for the Mesoproterozoic, elevated levels of CO_2 and CH_4 have been proposed to provide the necessary warming to avoid enhanced glaciation [20]. While higher Mesoproterozoic CO_2 is consistent with geological records [63], recent research has cast doubt on elevated CH_4 concentrations during the Mesoproterozoic due to predicted fluxes into the atmosphere that are similar to present day fluxes or lower [21,22,68]. Disregarding anthropogenic emissions, methane (CH_4) is currently produced on Earth primarily through biological pathways [22]. However, there are no direct indicators of CH_4 levels before the Pleistocene (>2.580 Myr ago) [22], so its concentration through geological time has generally been inferred through modelling. Laakso & Schrag [22] suggested Proterozoic methane levels no greater than 1 ppmv, and Olson *et al.* [21] suggested CH_4 concentrations were unlikely to exceed 10 ppmv, as did Daines & Lenton [68]. This is in contrast

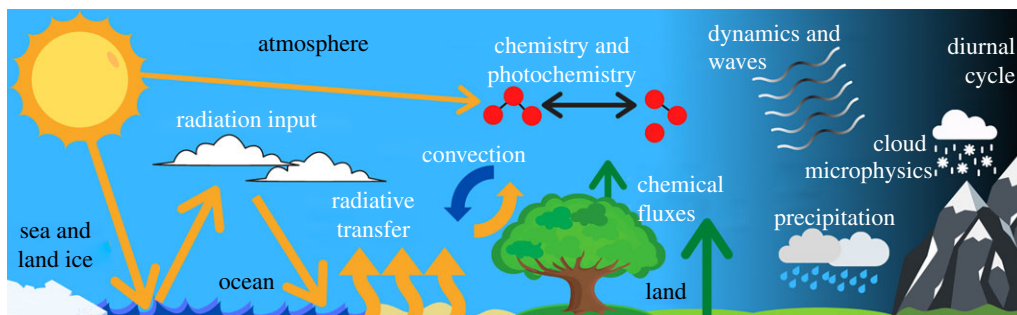


Figure 2. A schematic of the WACCM6 Earth System Model. In this work, WACCM6 made use of a fully interactive ocean model, as well as land-ice, sea-ice, land and atmosphere models. WACCM6 has fully coupled chemistry and physics, a state-of-the-art moist physics scheme, and simulates up to roughly 140 km in altitude in the pre-industrial atmosphere.

with the suggestion of 100–300 ppmv by Pavlov *et al.* [20], which was proposed to solve this Proterozoic Faint Young Sun Paradox.

Much of the work regarding the temporal variation of the O₃ layer and any influence on biological habitats has been achieved through one-dimensional atmosphere modelling studies [56–58,69]. For the first time, we use a whole atmosphere chemistry-climate model to simulate three-dimensional O₃ variations with changing O₂ concentrations under Proterozoic and Phanerozoic conditions applicable to the Earth. Owing to the uncertainty in O₂ concentrations during these geological eons, we simulate a range of possible O₂ levels (0.1% PAL to a maximum of 150% PAL) since the beginning of the Proterozoic to the pre-industrial atmosphere. We demonstrate oxygen's three-dimensional influence on the O₃ layer (its magnitude and spatial variation) and discuss how this affects habitability (the ability for life to survive on the surface) estimates. We then determine the effects that lower O₂ and O₃ quantities have on the chemical lifetime of CH₄, describing how the Proterozoic Faint Young Sun Paradox is now more difficult to solve. We also determine the differences that arise when using a three-dimensional chemistry-climate model for modelling paleoclimates compared to one-dimensional modelling studies.

2. Atmospheric modelling using WACCM6

This work uses the most recent version of the Whole Atmosphere Community Climate Model—WACCM6 [70], which is a specific model configuration of the Community Earth System Model version 2 (CESM2).¹ A schematic of the model's capabilities is shown in figure 2. WACCM6 is a three-dimensional Earth System Model (ESM). The model couples together atmosphere, land, land-ice, ocean and sea-ice sub models. The atmosphere component in CESM2 has been updated for almost every physical regime since the previous iteration of CESM1. For instance, the code modelling moist physics and turbulence received a major update [71]. WACCM6 has 70 atmospheric layers, from a surface pressure of 1000 hPa to a pressure of 4.5×10^{-6} hPa, the latter of which corresponds to an approximate altitude of 140 km (the lower thermosphere) for the pre-industrial atmosphere [70]. Each simulation used a horizontal grid of $2.5^\circ \times 1.875^\circ$ (longitude \times latitude), and a 30 min time step. Previous versions of WACCM have been used for a variety of purposes, such as simulating climate change between the industrial revolution and the twenty-first century [72], as well as investigating the effects of solar flares on the middle atmosphere [73]. This same model version has also previously been used in the context of exoplanets [74–77]. Our work is the first time the WACCM configuration of CESM has been used to model the Proterozoic Earth and calculate how the O₃ column varies with O₂ concentration, although we note that Chen *et al.* [77] did simulate Proterozoic-like O₂ concentrations for Earth-analogue exoplanets.

We ran 12 different simulations for this work (see table 1 for a summary). Our control simulation is a pre-industrial atmosphere (hereafter PI) in which pollutants and greenhouse gas concentrations approximate those of the year 1850. This simulation starts following a 300 year control simulation with fixed 1850 conditions. We vary the mixing ratio of O₂ over the range of possible values during the last 2.4 billion years following the Great Oxidation Event. These levels are 150%, 50%, 10%, 5%, 1%, 0.5% and 0.1% PAL. The standard WACCM6 pre-industrial baseline simulation initial conditions were altered

¹<http://www.cesm.ucar.edu/models/cesm2/>

Table 1. The 12 different simulations used for this work. There is a pre-industrial (PI) case and seven cases with varied O₂ levels. There are variations on the 1% PAL simulation, two with methane emissions (CH₄ em1 and CH₄ em0.1), and two with a 2 Gyr younger Sun, with pre-industrial CO₂ levels and four times the pre-industrial CO₂ levels, named YS and YS 4 × CO₂, respectively. The volume mixing ratio for O₂, f_{O_2} , is given in terms of present atmospheric level (PAL). The volume mixing ratio for N₂, f_{N_2} , is listed. The lower boundary condition (LBC) for CH₄ is shown, as well as the fixed lower boundary condition for CO₂ (f_{CO_2}). The flux of solar radiation at the top of the atmosphere, relative to today's solar constant (S_{\odot}) is given as S .

simulation name	f_{O_2} (PAL)	f_{N_2}	CH ₄ LBC	f_{CO_2}	S (S_{\odot})
PI	1.000	0.78	fixed 0.8 ppmv	280 ppmv	1.00
150% PAL	1.500	0.68	fixed 0.8 ppmv	280 ppmv	1.00
50% PAL	0.500	0.89	fixed 0.8 ppmv	280 ppmv	1.00
10% PAL	0.100	0.97	fixed 0.8 ppmv	280 ppmv	1.00
5% PAL	0.050	0.98	fixed 0.8 ppmv	280 ppmv	1.00
1% PAL	0.010	0.98	fixed 0.8 ppmv	280 ppmv	1.00
CH ₄ em1	0.010	0.98	5×10^{14} g yr ⁻¹ flux	280 ppmv	1.00
CH ₄ em0.1	0.010	0.98	5×10^{13} g yr ⁻¹ flux	280 ppmv	1.00
YS	0.010	0.98	fixed 0.8 ppmv	280 ppmv	0.86
YS 4 × CO ₂	0.010	0.98	fixed 0.8 ppmv	1120 ppmv	0.86
0.5% PAL	0.005	0.98	fixed 0.8 ppmv	280 ppmv	1.00
0.1% PAL	0.001	0.98	fixed 0.8 ppmv	280 ppmv	1.00

to produce each of these simulations, where the only variable change is the oxygen mixing ratio at the lower boundary—see figure 3 for the O₂ mixing ratio profiles. For each of these simulations, the mixing ratios of the following chemical species were held constant at the surface: O₂ (varied as in table 1), CH₄ (0.8 ppmv), CO₂ (280 ppmv), N₂O (270 ppbv) and H₂ (500 ppbv). Other species, such as O₃ and OH were left to evolve chemically. The simulated atmospheres have a surface pressure of 1000 hPa, and in each simulation in which the mixing ratio of O₂ is decreased, N₂ is increased to maintain a 1000 hPa surface pressure. Each of these simulations uses a modern day solar spectrum.

Recent work on the bi-stability of oxygen in Earth's atmosphere suggests that oxygen levels between $3 \times 10^{-6}\%$ and 1% the present atmospheric level of O₂ are unstable on geological timescales [16]. The lowest O₂ concentration we simulated was 0.1% PAL. The 0.5% PAL and 0.1% PAL concentrations may not be relevant for long periods of time (that is, geologically speaking), however, this depends on oxygen's relative atmospheric flux and destruction. We note that such mixing ratios could be relevant for shorter periods of time, and such concentrations could be stable on possible exoplanet atmospheres, so we include the 0.1% PAL and 0.5% PAL simulations for this reason.

Variations on the 1% PAL simulation were also run. While some research has advocated for a methane supported greenhouse during the Proterozoic [20,78], recent research has argued that CH₄ in the Proterozoic atmosphere was lower, with mixing ratios similar to or lower than present day due to aqueous oxidation [21,68] or due to a low efficiency in converting organic carbon to CH₄ [22]. To test the impact of variable CH₄ concentrations, we ran a 1% PAL of O₂ simulation with CH₄ emissions where the flux of CH₄ to the atmosphere is the approximate modern day flux of 5×10^{14} g yr⁻¹ (CH₄ em1), and a simulation with a reduced CH₄ flux of 5×10^{13} g yr⁻¹ (CH₄ em0.1), which is based on suggested lower fluxes of CH₄ to the atmosphere during the Proterozoic by Laakso & Schrag [22]. We also ran two simulations using a theoretical spectrum of the Sun 2 billion years ago [79] to investigate the impact of a less luminous younger Sun. We used an existing solar evolution model [79] to produce the solar spectrum at 2 Gyr before present. The model can produce theoretical spectra for the Sun between 4.4 Gyr in the past and 3.6 Gyr in the future. The model is valid between 0.1 nm and 160 μm, and so we extend the model further into the far infrared by modelling the Sun in this region as a blackbody. The spectrum from the solar evolution model was re-binned² while conserving flux, to ensure that the new spectrum was interpolated onto the WACCM6 spectral irradiance grid. This young Sun's modelled total energy output was 14% less than the present Sun, with a weaker ultraviolet flux (the UV range was assumed to be between 10 nm and 400 nm) by a factor of 1.19, and

²Using a Python tool called SpectRes [80].

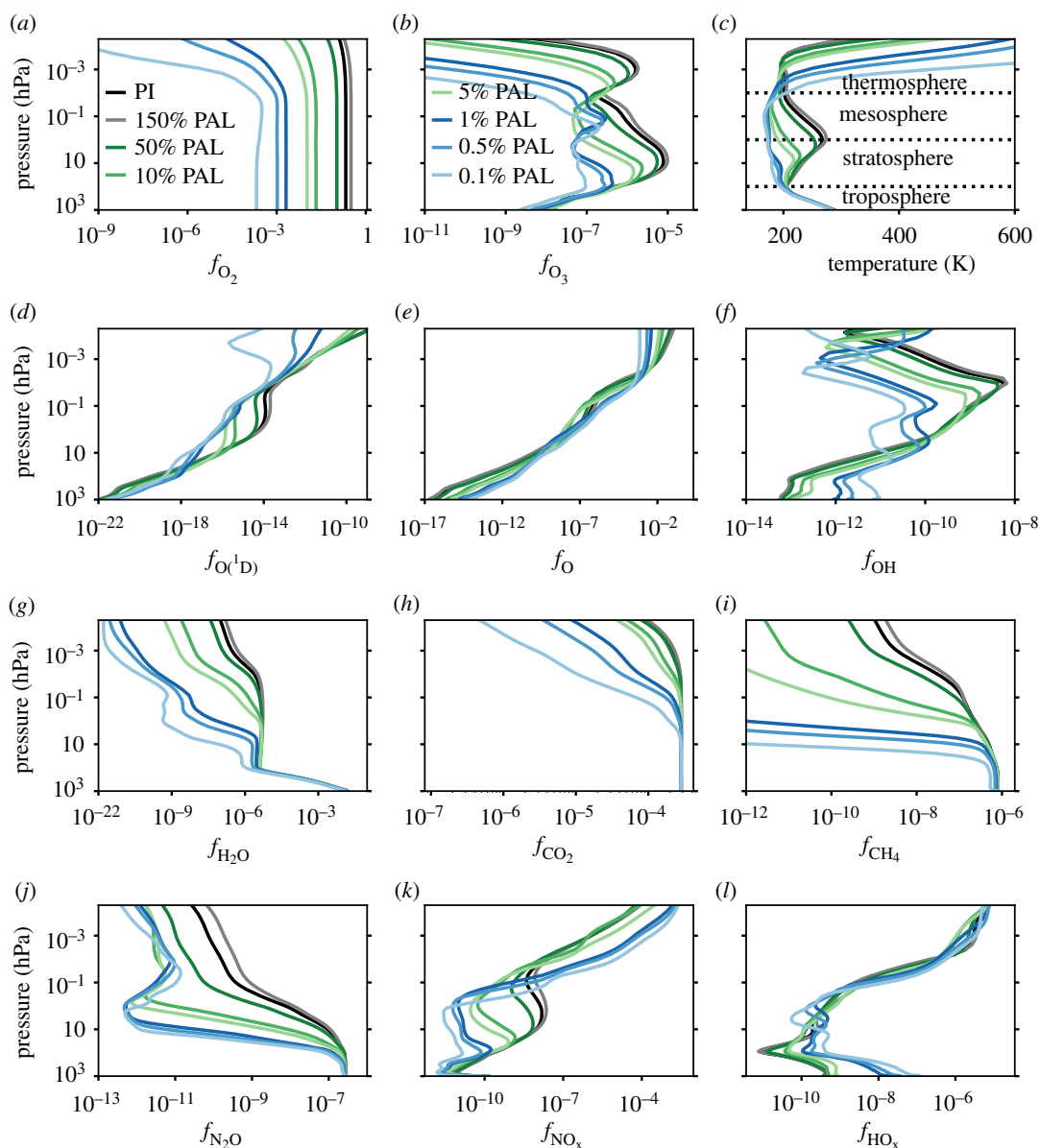


Figure 3. Selected time-averaged global mean atmospheric profiles output from the WACCM6 simulations are plotted. The PI (black), 150% PAL (grey), 50% PAL (dark green), 10% PAL (green), 5% PAL (light green), 1% PAL (dark blue), 0.5% PAL (blue) and 0.1% PAL (light blue) simulations are shown. PAL means relative to the present atmospheric level of O_2 which is 21% by volume. Mixing ratios for atmospheric constituents are shown for O_2 (a), O_3 (b), $O(^1D)$ (d), O (e), OH (f), H_2O (g), CO_2 (h), CH_4 (i), N_2O (j), NO_x (k), and HO_x (l). The PI atmospheric layers are indicated by black dotted lines alongside the temperature profiles in panel (c).

a stronger extreme ultraviolet flux (the extreme ultraviolet wavelength range was assumed to be between 10 nm and 91 nm) by a factor of 2.98. This younger Sun spectrum was used as input to the YS simulation and the YS $4 \times CO_2$ simulation. The YS simulation has a surface mixing ratio of 280 ppmv of CO_2 (the same as the PI simulation), while the YS $4 \times CO_2$ simulation has a surface mixing ratio of 1120 ppmv of CO_2 , to offset the fainter Sun.

In each simulation other than the PI case, new minimum mixing ratios for O_3 and CH_4 , both set at 10^{-12} , were set to 10^{-17} and 10^{-25} , respectively. A constant mixing ratio condition for O_2 at the lower boundary was imposed for the 0.5% and 0.1% PAL simulations because surface O_2 decreases below these scaled values without the imposed boundary condition. At 1% PAL and above, this does not occur on the time scales simulated.

The upper boundary conditions at 4.5×10^{-6} hPa are even more uncertain than the lower boundary conditions because there are fewer geological proxies for the upper atmosphere. Micrometeorites have

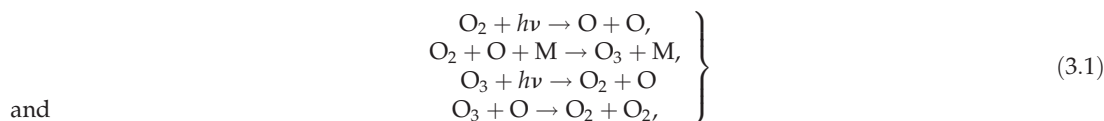
been used to constrain the composition of the lower and upper atmosphere in the Neoproterozoic 2.7 Gyr ago [81–84]. For example, Tomkins *et al.* [81] and Rimmer *et al.* [82] estimated high (approx. 0.21) upper atmospheric O₂ concentrations, and Payne *et al.* [83] and Lehmer *et al.* [84] argued instead for high (possibly with mixing ratios of greater than 0.23) atmospheric CO₂ concentrations up to the homopause. Pack *et al.* [85] used micrometeorites to show that Earth's modern atmospheric O₂ is isotopically homogeneous below the thermosphere. Nonetheless, we do not know of any upper atmospheric constraints for the Proterozoic. We therefore ran many perturbation experiments to select upper boundary conditions in each simulation for H₂, H, H₂O, CH₄, O, O₂ and N that created smooth, consistent profiles in the thermosphere. However, we found that the upper boundary condition does not affect the atmosphere below 5×10^{-5} hPa, as long as the upper boundary condition is not unreasonably large (for example, using a mixing ratio of 0.1 for water vapour would be unrealistic—see figure 3). The minimum pressure in our figures is thus cut to 5×10^{-5} hPa. It is important to note that the choice of upper boundary conditions does not impact on our conclusions.

Simulations were run until the annual cycle in total hydrogen repeats for 4 years, and there were no significant surface temperature trends in the simulations where only oxygen was changed. All results presented are time-averaged means that were from the last 4 years of each simulation. Zonal means and global means are area weighted.

3. Results

3.1. The oxygen–ozone relationship

An oxygenated atmosphere enables the photochemical production of O₃, which is primarily produced in the tropical stratosphere, where incoming sunlight photodissociates O₂ and produces an oxygen atom (O). O combines with O₂ and any third body (M) to form O₃. This O₃ molecule can absorb ultraviolet (UV) radiation, dissociating into O and O₂. O₃ can also react with O to produce two O₂ molecules. This is known as the Chapman cycle [86]:



where $h\nu$ represents a photon, h is Planck's constant and ν is the frequency of the photon. However, the chemistry of O₃ is more complicated than this, with catalytic cycles involving nitrogen, hydrogen and halogen species playing an important role in destroying O₃ molecules [87,88]. WACCM6 includes such chemical reactions [89,90].

Figure 3 shows how imposing Proterozoic O₂ levels leads to striking changes in the chemical structure of the atmosphere. The maximum O₃ volume mixing ratio in the 0.1% PAL simulation (0.24 ppmv) is ≈ 40 times lower than the maximum in the PI simulation (9.99 ppmv). A decrease in O₂ concentration results in a reduction in O₃ column density, which then enables increased ultraviolet flux in the lower atmosphere and increased photolysis rates. This reduces the mixing ratios of important greenhouse gases such as H₂O, CH₄, N₂O and CO₂: from the PI simulation to the 0.1% PAL simulation, at 0.1 hPa, the time-averaged mean volume mixing ratios for these species have been reduced by factors of 8.4×10^3 , $\sim 10^{18}$, 51 and 3.5, respectively.

For an atmosphere with a surface pressure of 1000 hPa, where O₂ has been replaced by N₂ to maintain the surface pressure, a greater wavelength range shortward of the visible continuum can penetrate the lower atmospheric levels. For instance, the Lyman- α line (121.6 nm), which is primarily absorbed by O₂ and usually only reaches approximately 80 km, can now photolyse H₂O and CH₄ at lower altitudes.

Increased tropospheric photolysis of H₂O, given by the reaction



and increased photolysis of O₃, represented by the reaction



result in the production of more OH and O(¹D), which are key drivers of atmospheric chemistry. OH is increased at the surface from a volume mixing ratio of 6.2×10^{-14} to 6.9×10^{-12} between the PI case and

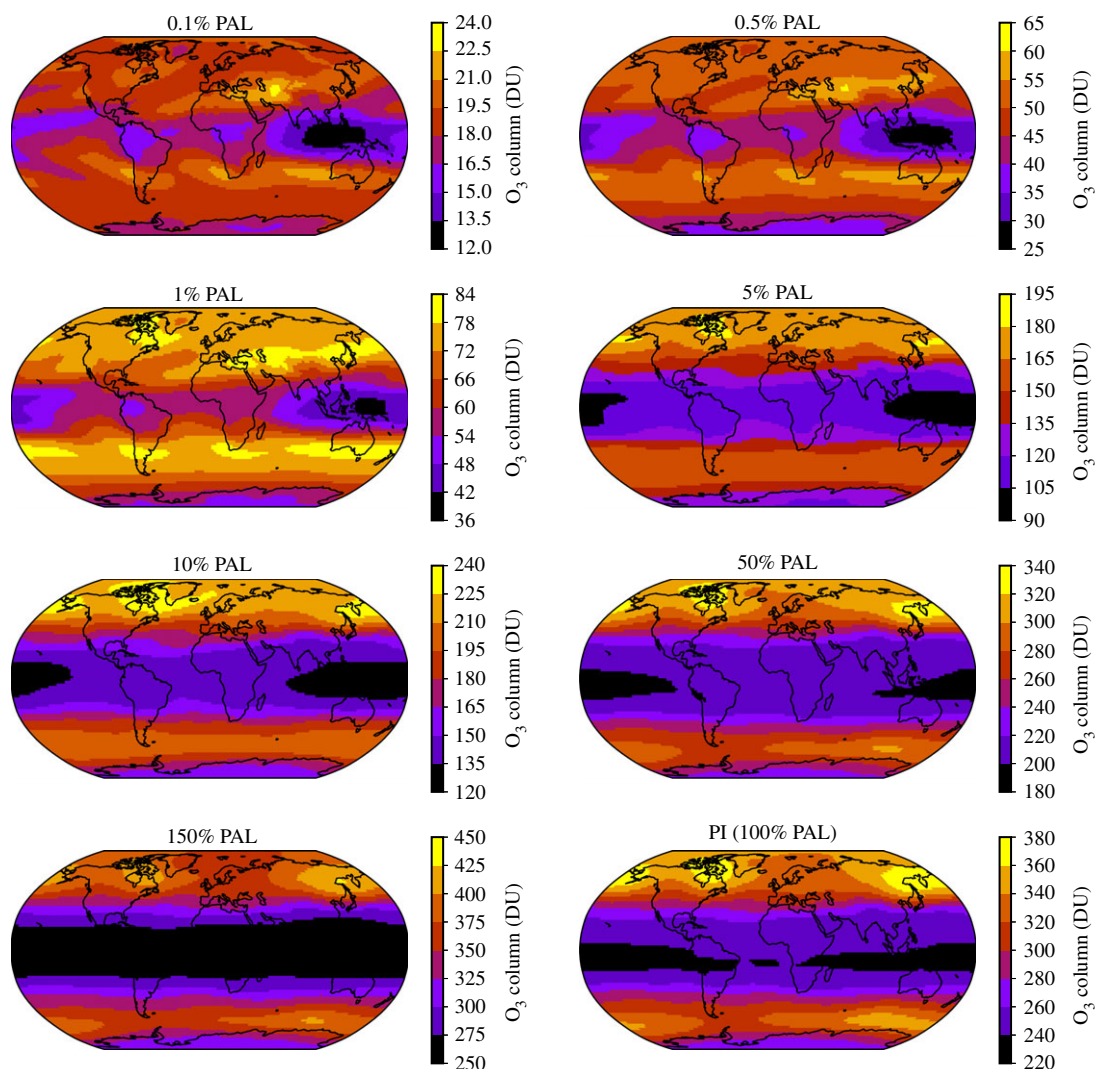


Figure 4. The O_3 column is plotted (superimposed on Earth's surface) in Dobson Units (DU) for the PI atmosphere and all the atmospheres where only oxygen concentrations were changed. Note the different scales on the colourbars. The tropics straddle either side of the equator, with the poles at the top and bottom of the two-dimensional maps, and the extratropics at intermediate latitudes.

the 0.1% PAL case. As a result of oxidation by OH and $O(^1D)$, the loss rate of CH_4 from the troposphere is increased by the following two reactions:



and



There is more stratospheric HOx ($HOx = H + OH + HO_2 + 2 \cdot H_2O_2$) as O_2 decreases which leads to further O_3 destruction. In the troposphere and lower stratosphere, each component of HOx is increased because the reaction



leads to reactions that then produce more HO_2 and H_2O_2 .

By contrast, NOx ($N + NO + NO_2$) is generally lower in the troposphere and stratosphere as O_2 is decreased. Usually, stratospheric N_2O gives rise to more NOx through the reaction



[91]. When O_2 is reduced, tropospheric and stratospheric photolysis of N_2O instead produces $O(^1D)$ and N_2 , and the path to NOx creation becomes increasingly limited with increasing photolysis.

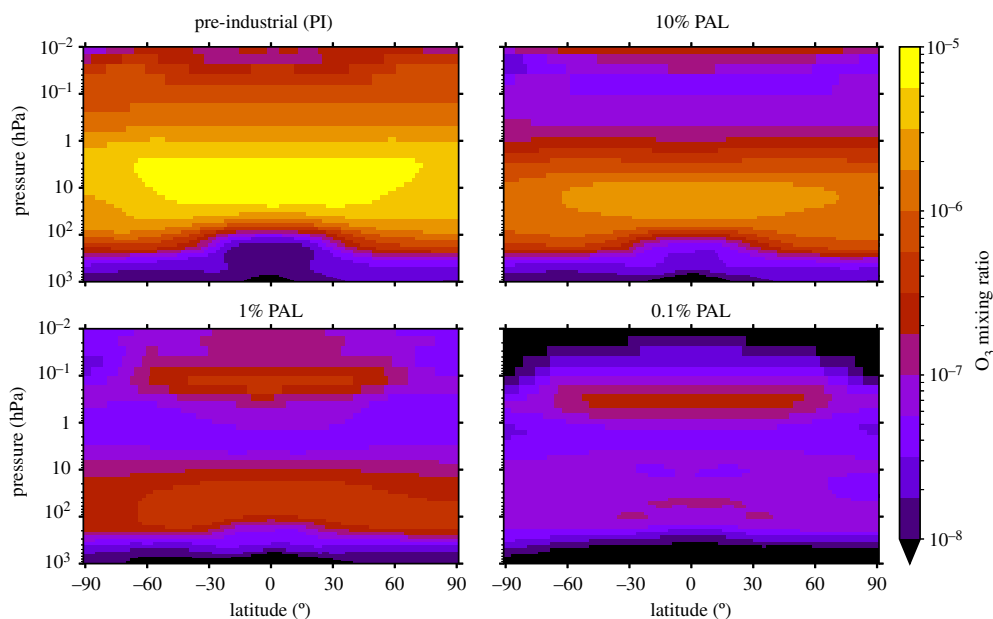


Figure 5. The four panels show the O_3 mixing ratio structure in the zonal mean (longitudinal mean) between the surface and 0.01 hPa, for the PI, 10% PAL, 1% PAL and 0.1% PAL atmospheres. The North Pole is at 90° latitude, the equator at 0° , with the South Pole at -90° latitude. The secondary night-time O_3 peak is not visible for the PI and 10% PAL atmospheres as it lies above 0.01 hPa.

The Earth's present-day O_3 column varies geographically depending on incident sunlight and the Brewer–Dobson circulation [92]. The Brewer–Dobson circulation—characterized by upwelling in the tropical stratosphere, followed by poleward movement of air parcels, then downwelling in the extratropical stratosphere—distributes O_3 to higher latitudes [92,93]. The O_3 layer thus provides varying levels of UV protection across the Earth's surface which varies with season and latitude. Figure 4 shows the annual mean geographical variation across Earth's longitudinal and latitudinal grid. The simulated global mean total O_3 column for the PI atmosphere case is 279 Dobson Units ($1 \text{ DU} = 2.687 \times 10^{20} \text{ molecules m}^{-2}$), decreasing to O_3 columns of 169 DU, 66 DU and 18 DU for the 10% PAL, 1% PAL and 0.1% PAL simulations, respectively. As O_2 decreases, there is a clear disruption in the pre-industrial O_3 distribution. Instead of the thick equatorial band of low O_3 levels in the PI atmosphere, the simulations which have oxygen levels $\leq 5\%$ PAL have annual mean equatorial O_3 holes over the Pacific ocean and the Indian ocean.

Figure 5 shows the zonal mean structure of O_3 for the PI, 10% PAL, 1% PAL, and 0.1% PAL simulations. The stratospheric O_3 layer shifts in terms of altitude, shape and latitudinal variation, as does the secondary night-time O_3 layer. O_3 can be seen to trace the pressure-varying tropopause in the PI atmosphere. This is less apparent as oxygen decreases.

Displayed in figure 6 is the variation of the total O_3 column (and thus the modulation of surface UV fluxes) with atmospheric O_2 mixing ratio. The PI simulation recovers the pre-industrial O_3 column in both magnitude and latitudinal variation. At several O_2 concentrations, we report lower total O_3 columns compared to previous one-dimensional and three-dimensional work [56–58,69,94]. In the 10% PAL case, the mean column is approximately 1.46, 1.57, 1.76 and 2.43 times smaller when compared to Way *et al.* [94], Segura *et al.* [58], Kasting & Donahue [57] and Levine *et al.* [56], respectively. For the 1% PAL case, the mean O_3 column is approximately 1.83, 1.87, 2.24 and 2.89 times smaller when compared with Way *et al.* [94], Segura *et al.* [58], Kasting & Donahue [57] and Levine *et al.* [56], respectively. Also for the 1% PAL case, if we were to include minimum time-averaged values (likely at the equator where UV irradiation is highest), then the discrepancy is larger and the minimum O_3 column is 2.97, 3.04, 3.63 and 4.68 times smaller compared to mean O_3 columns from Way *et al.* [94], Segura *et al.* [58], Kasting & Donahue [57] and Levine *et al.* [56], respectively. We also show, along with the previous one-dimensional result from Kasting & Donahue [57] and the three-dimensional result from Way *et al.* [94], that O_3 levels consistently rise with increasing O_2 levels, rather than plateauing and decreasing between 0.1% PAL and 1% PAL, which previous one-dimensional models have reported [69].

The O_3 column is not just determined by O_2 . It depends on many factors, including other chemical species present in the atmosphere, the flux of incoming solar radiation, and atmospheric circulation. In

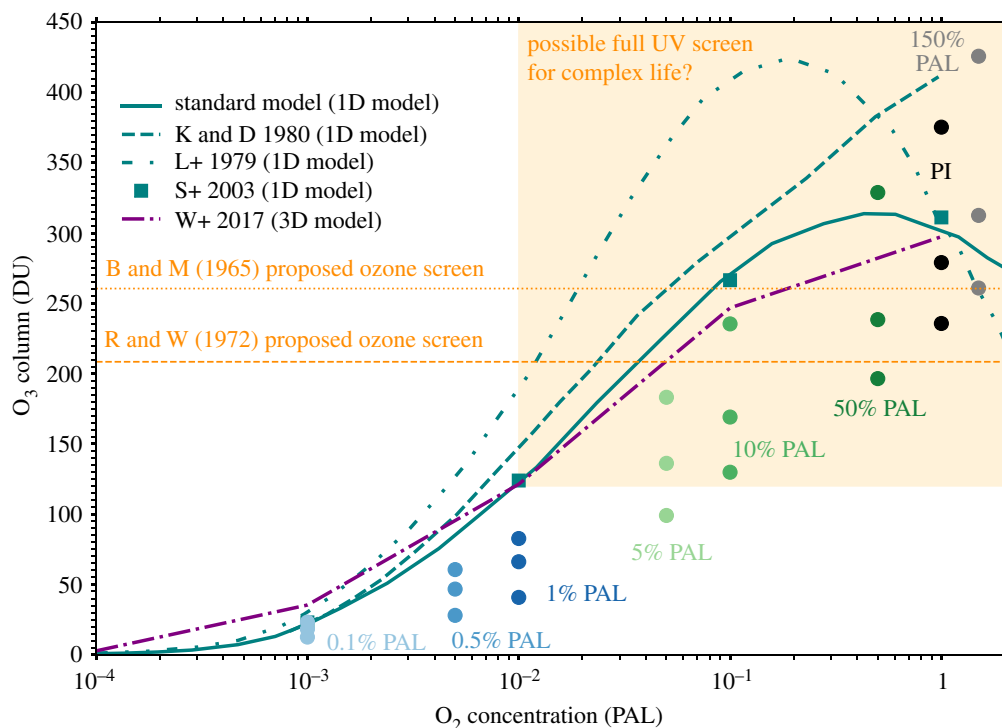


Figure 6. Shown by the circles (in the same colour scheme as figure 3) are the maximum, mean and minimum time-averaged O_3 columns from the varied O_2 simulations which are compared to the mean values from previous one-dimensional [56–58,69] modelling in teal, and three-dimensional [94] modelling in purple. Note that the data by Segura *et al.* [58] are indicated by the square points with no associated line. Indicated in orange shading is a proposed full UV screen, when taking into account literature assumptions (see discussion §4.1) that levels of O_2 at 1% PAL or higher form a fully-shielding O_3 layer. Also indicated by the orange dashed and orange dotted lines are the full UV shielding O_3 screens proposed by Berkner & Marshall [95] and Ratner & Walker [96], respectively.

figure 7, we show the impact on the O_3 column when we vary the CH_4 flux (and thus its mixing ratio), the solar spectrum, and increased CO_2 concentrations, in order to better simulate Proterozoic conditions. Using a spectrum of a younger Sun, which has a lower incident flux in the wavelength region that destroys O_3 , the O_3 column is increased by ≈ 10 DU. Relative to the YS simulation, the O_3 column in the YS $4 \times CO_2$ case is greater by ≈ 5 DU. This is because increased CO_2 concentrations cool the stratosphere, mesosphere and lower thermosphere, and O_3 production is temperature dependent (i.e. cooler temperatures result in faster O_3 production). Lower CH_4 mixing ratios act to reduce the O_3 column by ≈ 5 DU because there is more $O(^1D)$ and OH available to destroy O_3 that would otherwise have reacted with CH_4 molecules. In all cases with 1% PAL of O_2 , the mean O_3 column values are lower than previous predictions.

3.2. The proterozoic Faint Young Sun problem

The Faint Young Sun Paradox is the problem associated with the early Sun outputting less total energy, yet the surface temperatures of Earth remaining high enough for liquid water to exist [66]. While the Faint Young Sun Paradox may have been solved for the Archean climate [67], the question of how the Earth maintained a mostly ice-free surface throughout most of the Proterozoic remains to be answered [21,63]. Some studies have suggested that an elevated CH_4 greenhouse can solve this problem [20,78]. In contrast with this, more recent work has suggested otherwise [21,22,68]. Here we explore possible methane concentrations during the Proterozoic.

The chemical lifetime of a molecule is its mean lifetime before it is destroyed. Reducing O_2 vastly reduces atmospheric chemical lifetimes for several important species, including the lifetime of CH_4 (τ_{CH_4})—see figure 7. The lifetime of any molecule throughout the atmosphere varies depending on photochemical destruction rates and chemical reaction rates, as well as transport of the molecule. We present global mean τ_{CH_4} profiles varying with atmospheric pressure. The actual lifetime of a CH_4 molecule will vary depending on where it is produced and to where it is transported.

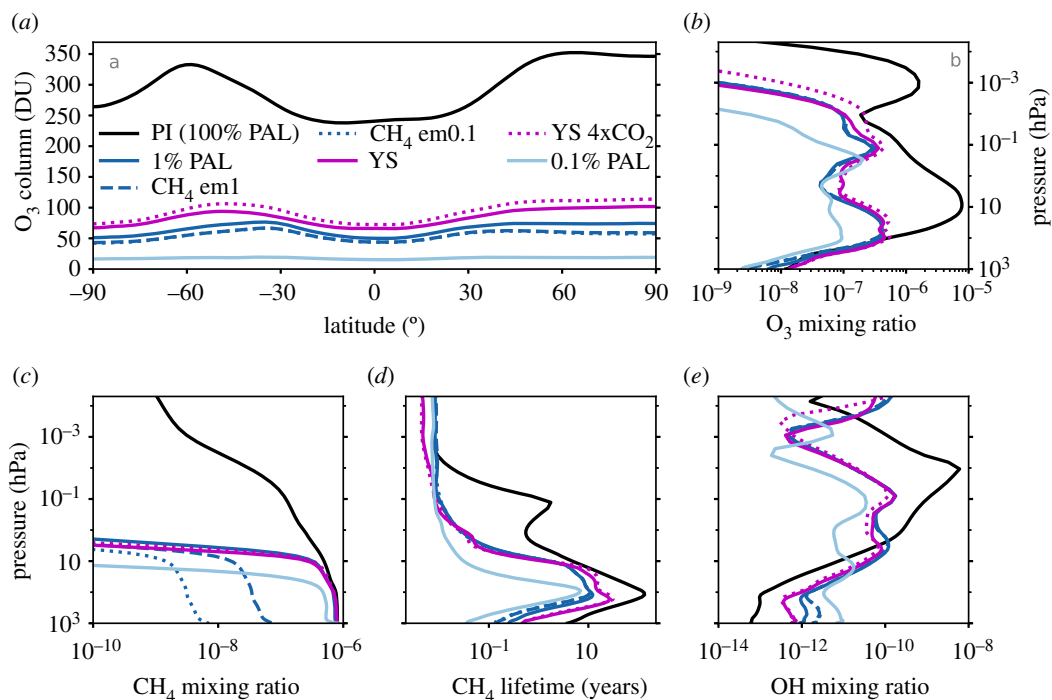


Figure 7. Mixing ratio and chemical lifetime of CH₄. In all panels, the PI (black), 1% PAL (dark blue), 0.1% PAL (light blue), CH₄ em1 (dark blue dashed), CH₄ em0.1 (dark blue dotted), YS (magenta) and YS 4 × CO₂ (magenta dotted) simulations are shown. The latitudinal variation of the O₃ column is shown in panel *a*, and the O₃ mixing ratio profile is shown in *b*. The CH₄ mixing ratio is plotted in panel *c*, and the atmospheric chemical lifetime of CH₄ (τ_{CH_4}) is plotted in panel *d*. Note that the CH₄ lifetime depends on the number density of CH₄ and its loss rate. Finally, panel *e* displays the OH mixing ratio.

Table 2. The chemical lifetime of CH₄ (τ_{CH_4}) at the surface is given in years. This surface lifetime is then compared to the surface lifetime of CH₄ in the PI atmosphere ($\tau_{\text{CH}_4, \text{PI}}$) to calculate a ratio between them ($\tau_{\text{CH}_4} / \tau_{\text{CH}_4, \text{PI}}$).

simulation name	surface τ_{CH_4} (yr)	surface $\tau_{\text{CH}_4} / \tau_{\text{CH}_4, \text{PI}}$
PI	3.813	1.000
150% PAL	4.044	1.061
50% PAL	3.442	0.903
10% PAL	2.661	0.698
5% PAL	1.983	0.520
1% PAL	0.256	0.067
CH ₄ em1	0.155	0.041
CH ₄ em0.1	0.140	0.037
YS	0.473	0.124
YS 4 × CO ₂	0.454	0.119
0.5% PAL	0.126	0.033
0.1% PAL	0.037	0.010

Table 2 shows the surface τ_{CH_4} values for all the simulations. τ_{CH_4} is 3.8 years at the surface for the PI case and just 13 days for the 0.1% PAL case. The lifetime of CH₄ increases with height in the troposphere due to temperature-dependent chemical loss, before it decreases in the stratosphere due to photochemical loss, and oxidation with either OH or O(¹D). Each of the varied O₂ simulations have a constant surface CH₄ mixing ratio. In reality, a flux to the atmosphere sustains a constant, or time-varying, surface mixing ratio. Despite using a constant mixing ratio, we can predict the flux that would be needed to sustain CH₄ at 0.8 ppmv in each simulation, as τ_{CH_4} does vary at the lower boundary in each case. The ratio between

the surface lifetimes is the inverse of the ratio of the surface fluxes. To illustrate, the ratio between the 1% PAL τ_{CH_4} and the PI τ_{CH_4} is 0.067, meaning that a flux increase of $1/0.067 \approx 15$ compared with the pre-industrial flux would be needed to sustain surface CH_4 at 0.8 ppmv in the 1% PAL simulation. All CH_4 lifetime ratios are given in table 2.

In the low O_2 simulations, a greater in magnitude increase in CH_4 flux, especially between 10 and 100 times the pre-industrial day flux, is unrealistic. In fact, it is possible that fluxes were lower than in the present day and could have been less than or equal to 0.1 times the present-day emissions [22]. In the CH_4 emissions simulations, CH_4 is reduced at the surface to ≈ 0.08 ppmv and ≈ 0.007 ppmv for the CH_4 em1 and CH_4 em0.1 simulations, respectively. So, it is likely that CH_4 fluxes to the atmosphere during the Proterozoic were either reduced compared to the pre-industrial flux [22], or they were not much greater [21,68], and that the atmospheric chemical lifetime of CH_4 was reduced due to a diminished O_3 column. Therefore, CH_4 would not have been a significant greenhouse gas during the Mesoproterozoic.

4. Discussion

4.1. Habitability and increased UV radiation

Our results show that previous one-dimensional and three-dimensional modelling may have overestimated Earth's mean O_3 column for atmospheric O_2 mixing ratios between 0.5% PAL and 50% PAL, with these mixing ratios having relevance for both the Phanerozoic and Proterozoic. In this section, we explore the potential implications for habitability during these time periods.

Assessing surface habitability is not simple. It depends on many factors, including the temperature and pressure at the surface, and also the type of life in the environment that is being evaluated. For instance, humans cannot survive in conditions where bacterial extremophiles flourish [97]. The discussion of habitability here will be limited to UV radiation, which has varying effects depending on the organism considered (note that many organisms have developed strategies to avoid excessive UV damage, as well as repair mechanisms to mitigate its effects [98–101]). Although microbial life is known to survive stronger than ambient UV irradiation [97,102,103], many animals and plant species are impacted by high doses of UV radiation, resulting in infertility [59], cell death [104] and increased mortality rates [105–107], with UV radiation considered an environmental stressor [108].

Higher surface UV fluxes during the Early Paleozoic or throughout the Proterozoic could have exerted an ecological selection pressure for organisms [109–111]. Indeed, some mass extinction events have been linked to reduced O_3 columns that have resulted in high UV-B fluxes [59,60,112,113]. Several decades ago, Berkner & Marshall [95] suggested that UV radiation could have prevented the colonization of dry land, but more recent literature suggests this was unlikely [55,62,102,111,114,115]. However, UV radiation may have still played a role in the subsequent evolution of life on land once it was colonized [59,60,116–118], just as stratospheric O_3 depletion in the last few decades, which has resulted in increased surface UV flux, has affected animals and plants in the Southern Hemisphere [119,120].

Life in the oceans experiences lower fluxes of UV radiation compared with life on land because water attenuates UV radiation [121]. There is ample evidence of life existing in the Proterozoic oceans ([11,19] and references therein), yet this does not mean that life in the photic zone (the topmost layer of the ocean which is illuminated by sunlight) would have been unaffected by UV radiation.

Photosynthesis may have been inhibited under the UV irradiance of the Proterozoic [115]. In the modern ocean, it was estimated by Smith *et al.* [122] that primary productivity³ reduced by 6–12% under the Antarctic ozone hole. A decrease in growth rates and an increase in cell death was reported in phytoplankton by Llabrés & Agustí [123] under ambient UV-B radiation compared to no UV-B radiation. Additionally, Bancroft *et al.* [124] found through meta-analysis a widespread, overall negative effect on aquatic ecosystems from UV-B radiation, noting that the effects vary and are organism dependent. Llabrés *et al.* [125] performed a larger meta-analysis on marine biota, finding 'protists, corals, crustaceans and fish eggs and larvae' were the 'most sensitive' to increased levels of UV-B radiation. Mloszewska *et al.* [126] argued that primary productivity from cyanobacteria would have remained low until a permanent ozone screen formed at 1% PAL, citing one-dimensional modelling studies [58,127] in this assertion.

For O_2 concentrations between 0.5% PAL and 50% PAL, the total mean O_3 column quantities in our three-dimensional simulations are reduced by a factor of 1.2–2.9 times when compared to prior one-

³Primary productivity is the rate at which organic compounds are produced from CO_2 , usually through photosynthesis.

dimensional and three-dimensional simulations [56–58,69,94]. This is maximized when considering the 1% PAL simulation minimum, with the minimum O₃ column reduced between 3 and 4.7 times when compared to previous mean O₃ column estimations. We compare the minimum here because the minimum is usually associated with the equatorial regions (figure 4), which cover a large proportion of the Earth's surface, receive the highest amounts of solar radiation, and are thus important for habitability predictions.

Whilst these reductions do not seem like large numbers, because O₃ reduces UV fluxes through a power law [128], an apparently small change in O₃ can lead to a large change in surface UV fluxes. For example, Black *et al.* [61] studied O₃ depletion resulting from the Siberian Traps eruptions, calculating O₃ columns ranging between ≈ 55 and ≈ 145 DU, with estimated increases in biologically damaging UV-B radiation between 5 and 50 times that of present day fluxes. Rugheimer *et al.* [129] modelled modern Earth and Earth in the past. They reported an 8.8 factor decrease in O₃ column (196.9 DU \rightarrow 22.4 DU) between their modern Earth case and their case of Earth 2 Gyr ago. Despite total top of atmosphere UV-B (280–315 nm) and UV-C (100–280 nm) radiation decreasing 2 Gyr ago in their simulations by 1.27 and 1.29 times, respectively, this O₃ reduction increased biologically damaging UV fluxes by 41.3 times, with surface UV-B and UV-C fluxes increasing by a factor of 2.74 and 2×10^{13} , respectively. Segura *et al.* [58] report an O₃ column of 266 DU in a 10% PAL atmosphere, whilst we report a minimum of 130 DU at 10% PAL. Segura *et al.* [58] had a mean O₃ column of ≈ 124 DU, but instead at 1% PAL rather than 10% PAL. For these two atmospheres (10% PAL \rightarrow 1% PAL), they estimated that UV-B and UV-C surface fluxes increased by 2.08 times and 4437.5 times, respectively. The discrepancy between our simulations and prior simulations matters when estimating the habitability of a planet or exoplanet. Even the lower estimates in the literature, that suggest 0.5% PAL of O₂ is required to produce an effective O₃ screen [115], calculate UV attenuation based on O₃ column estimates from the one-dimensional model used by Kasting & Donahue [57]. At 0.5% PAL, our mean and minimum O₃ columns (45 and 30 DU) are 2.2 and 3.3 times lower than the calculated value of 100 DU by Kasting & Donahue [57].

Reasoning regarding the evolutionary impact of the O₃ layer and associated UV fluxes has generally been based on converged atmospheric simulations from one-dimensional models [56,57,69], which estimate that roughly 1% of the present atmospheric level of O₂ gives rise to an O₃ layer that shields the biosphere [130]. This was originally based on passing the threshold for full UV screen limits of ≈ 210 DU proposed by Berkner & Marshall [95] and ≈ 260 DU proposed by Ratner & Walker [96]. More recently, atmospheric [16,22], biogeochemical [36,131], biological [55,126,132], and astrobiological/exoplanet work [74,131,133–137] have cited one-dimensional results in figure 6, often with the statement that at least 1% PAL of O₂ is needed to establish a full UV shield. Therefore, prior studies in figure 6 show that at 1% the present atmospheric level of O₂, the fully UV shielding range is between 120–185 DU for the mean O₃ column, whereas our 1% PAL simulation gives a mean O₃ column of just 66 DU, roughly half the lower end of the 120–185 DU range. Our simulations require 5% PAL of oxygen to reach a mean O₃ column of 136 DU, and 10% PAL to reach a mean of 169 DU and fully encompass the protective range when including our 10% PAL minimum of 130 DU. Thus, potentially 5–10 times more oxygen is required than previously thought to fully UV shield the biosphere, showing that the common assumption that 1% PAL of O₂ provides a full UV shield is potentially incorrect. Additionally, the real atmosphere is three-dimensional and varies temporally, and the O₃ layer can be influenced by biologically produced gases (e.g. O₂, CH₄), asteroid or comet impacts [138], solar activity and flares [73], as well as volcanic emissions [61].

Under reduced O₃ columns at O₂ mixing ratios between 0.5% PAL and 50% PAL, the surface and the photic zone would have received more UV radiation than previously believed. Consequently, the efficiency of photosynthesis throughout the low-O₂ range of the Proterozoic atmosphere could have been restricted, and UV fluxes may have acted as a stronger evolutionary variable for organisms that were susceptible to fluctuations in UV caused by O₃ column changes. The notion that there is a threshold above which a full-O₃ shield exists seems to simplify what is likely a complex interaction through Earth's oxygenated history between life's continuous evolution, and O₂, O₃ and UV radiation.

4.2. Origin of lower ozone columns in WACCM6

Why are our simulations predicting lower O₃ columns compared to previous work? Untangling the exact reasons and quantifying their magnitudes is difficult without a detailed model intercomparison. The following paragraph details possible reasons for discrepancies, which will require investigation with models to confirm.

Discrepancies with previous work may arise through the treatment of the diurnal cycle. Kasting & Donahue [57] and Segura *et al.* [58] used a solar zenith angle of 45° and multiplied photolysis rates by 0.5 to account for diurnal variation. This does not as accurately account for the temporal variation in O_3 throughout the atmosphere when compared to a three-dimensional model; Kasting & Donahue [57] reported that their O_3 profiles ‘represent an upper limit on the amount of O_3 present at a given oxygen level’. In addition, each model will have different chemical schemes and reaction rates, which have been updated in the four decades since the work of Kasting & Donahue [57]. Another possible reason for the O_3 column reduction is three-dimensional transport, which is difficult to treat appropriately in one-dimensional models. The full impact of three-dimensional transport (in particular the Brewer–Dobson circulation) and the diurnal cycle treatment is uncertain. For example, Way *et al.* [94] used a three-dimensional model (ROCKE-3D) and produced lower O_3 columns compared to previous one-dimensional work at 10% PAL, but roughly comparative O_3 columns at 0.1% PAL, 1% PAL and 100% PAL. We believe that we estimate lower O_3 columns compared to Way *et al.* [94] because their simulations did not have fully-coupled chemistry and physics, nor did they include radiation changes directly from O_2 changes. To isolate the reasons for the differences, future work is required to test our hypotheses. This could include incorporating three-dimensional model chemical schemes into one-dimensional chemical schemes, and vice versa, as well as setting a constant solar zenith angle in every grid box in three-dimensional models (multiplying photolysis rates by 0.5), and potentially adjusting heating rates for constant illumination.

A minor caveat in our study is that we have not simulated CO_2 mixing ratios above 1120 ppmv ($4 \times$ the pre-industrial CO_2 mixing ratio). We note that up to 2800 ppmv of CO_2 may be consistent with geological proxies during the Proterozoic [18,63]. Additional CO_2 cooling would act to slightly increase the O_3 column through the temperature dependence on chemical reactions and also contribute to the absorption of Lyman- α radiation in simulations with the very lowest O_2 concentrations. Higher CO_2 concentrations would reduce photolysis of H_2O and CH_4 in the upper atmosphere. However, since the absorption cross-section for O_2 at Lyman- α is ≈ 3 times greater than that of CO_2 [139–141] and Lyman- α fluxes in the lower atmosphere would remain very small, we expect that this does not affect our new estimates of the ozone column or methane’s negligible contribution to the Proterozoic greenhouse.

Our new results should not be treated as a real reconstruction of Earth’s past O_3 states, just as our results show taking one-dimensional O_3 calculations as ground truth is problematic; instead, one-dimensional O_3 calculations should be treated with caution. The lower O_3 columns predicted by our work have important consequences for life’s history on Earth, and the future estimation of habitability on exoplanets. At some point, Earth’s atmosphere is likely to pass through varied lower oxygenated states, including analogous states to those simulated here [142]. Following Ozaki & Reinhard [142], our simulations can be used as a further step for predictions of Earth’s future biosphere, its habitability, and observability. Moreover, paleoclimate modelling of the Earth that investigates specific climate events and geological processes will benefit from whole atmosphere three-dimensional chemistry-climate models that are coupled to dynamics. For instance, one-dimensional atmospheric models that investigate oxygenated exoplanet and paleo atmospheres could be tuned to replicate the lower O_3 column values. This tuning will also likely be applicable to oxygenated exoplanets orbiting other stellar spectral types, especially tidally locked M dwarf exoplanets, where simulating the dynamics is necessary to understand chemical transport between the day and night side of the planet.

4.3. Keeping the Mesoproterozoic ice-free

A reduced O_3 layer also affects the chemical composition of the troposphere, including the decreased abundance of CH_4 [21,57] caused by an increase in OH and $O(^1D)$. Methane is an important greenhouse gas, so we consider the Proterozoic greenhouse here.

The lack of evidence for glaciation during Earth’s Mesoproterozoic suggests a mostly ice-free surface during this era. Given that there is ice at Earth’s poles today, and during the Proterozoic there was less solar heating, then an ice-free surface without at least some increased greenhouse warming under a fainter Sun creates a contradiction, because one would expect more ice with a lower solar energy flux. To investigate this issue, we have simulated methane concentrations at varied O_2 concentrations and atmospheric CH_4 fluxes. We aim to answer the question, is it likely that a Mesoproterozoic greenhouse had substantial contributions from methane?

Three-dimensional simulations have shown that an ice-free surface can be sustained during the Mesoproterozoic if CO_2 is at 10 times its pre-industrial level and there is between 28 and 140 ppmv of CH_4 [63]. The mixing ratio of CH_4 at the surface in our fixed lower boundary condition simulations is

0.8 ppmv. Consequently, given the surface τ_{CH_4} values for the low O_2 cases, our results show that an approximate CH_4 flux increase (compared to present day) of a factor between 50 and 3500 is needed to reach levels of 28 ppmv during the Proterozoic (considering 10% PAL and 0.1% PAL, respectively), and five times these values to reach 140 ppmv.

Olson *et al.* [21] estimated that at 1% PAL of O_2 , net biogenic CH_4 would be $\approx 70 \text{ Tmol yr}^{-1}$, and the CH_4 mixing ratio would be at 33 ppmv. At 10% PAL of O_2 , methane production was estimated to be closer to 20 Tmol yr^{-1} , with CH_4 concentrations of 22 ppmv (their CH_4 predictions vary non-linearly with O_2 because of further screening by the O_3 layer with rising O_2 , and increased methanotrophic oxidation of CH_4). Laakso & Schrag [22], using a marine carbon cycling model after analysing organic carbon to CH_4 conversion efficiency at Lake Matano [143], calculated that for between 10^{-3} PAL and 10^{-1} PAL of oxygen during the Proterozoic, atmospheric methane mixing ratios were between 0.04 ppmv and 1 ppmv. They also estimated methane generation rates that did not exceed 50 Tmol yr^{-1} (similar to the pre-industrial flux) during the Precambrian, and that Proterozoic fluxes may have been 100 times lower than this. If we were to simulate atmospheric fluxes lower than 0.5 Tmol yr^{-1} , then CH_4 surface mixing ratios would drop below 8 ppbv for 1% PAL of oxygen. A Mesoproterozoic maximum of 10% PAL O_2 would allow for $\approx 10 \times$ more atmospheric CH_4 for equivalent atmospheric fluxes, but with the Proterozoic fluxes considered here, the CH_4 concentration would likely not exceed 1 ppmv.

Methane fluxes remain uncertain and disputed, with huge variation in literature predictions. For example, Cadeau *et al.* [144] refuted the conclusions reached by Laakso & Schrag [22] after analysis of biogeochemistry in Dziani Dzaha, a volcanic crater lake with similarities to expectations of the Proterozoic oceans (e.g. it has higher salinity compared to the modern oceans). Cadeau *et al.* [144] concluded that methanogenesis (anaerobic methane production) resulted in efficient mineralization of the lake's high primary productivity. In this argument, Cadeau *et al.* [144] also cited Fakhraee *et al.* [145], who evaluated that Proterozoic fluxes from the oceans to the atmosphere could have been as high as $60\text{--}140 \text{ Tmol yr}^{-1}$ ($9.6\text{--}22.4 \times 10^{14} \text{ g yr}^{-1}$), based on predicted low-sulphate Proterozoic oceans that were mostly anoxic. Furthermore, Lambrecht *et al.* [146] suggested that non-diffusive transport of CH_4 , such as the example of rising bubbles in Lake La Cruz that carry gases to the atmosphere composed of 50% CH_4 [147], should be considered in atmospheric models that simulate the production of CH_4 and its transport to the atmosphere. Regardless, in our simulations at 1% PAL of O_2 , 140 Tmol yr^{-1} ($22.4 \times 10^{14} \text{ g yr}^{-1}$) would not be a large enough flux to achieve CH_4 mixing ratios of 1 ppmv. As such, it is extremely unlikely that CH_4 concentrations could reach 28–140 ppmv (unless methane fluxes were larger than those found in recent literature), and thus the Mesoproterozoic could not have been kept in an ice-free state by a CH_4 supported greenhouse.

Could a photochemically produced haze layer prevent the reduction in methane we predict? Such a haze layer could contribute to an anti-greenhouse effect, i.e. it could cool the surface and reduce photolysis below this layer, increasing methane, which would then warm the surface. WACCM6 does not currently support the formation of organic haze from CH_4 photolysis, although a haze layer is unlikely to exist in our simulated atmospheres because the C/O ratio (liberated from CH_4 and Ox photochemistry) is $\ll 1$ in our simulations and it needs to be closer to approximately 0.5 to create a haze layer ([148,149] and references therein). This is because photolysis produces O radicals that prevent haze particle formation [148]. It has been found experimentally that haze particle production decreases as O_2 levels increase above 10^{-4} PAL, although haze particles are still produced [150]. At a pressure of $\approx 85\,000 \text{ Pa}$, 0.1% PAL of O_2 , 260 ppmv of CO_2 , and 158 ppmv of CH_4 , Hörst *et al.* [150] found a production of $\approx 1 \times 10^6$ haze particles cm^{-3} , such that at a C/O ratio of 0.75 (approx. 100 times greater than any C/O ratios we have simulated), these haze particles had a mixing ratio of roughly 5×10^{-14} . Furthermore, Olson *et al.* [21] found that hydrocarbon production from CH_4 photolysis during the Proterozoic would likely not result in a significant additional greenhouse contribution. When we include atmospheric CH_4 fluxes considering some recent estimated CH_4 atmospheric fluxes (table 1) [21,22], CH_4 concentrations are even lower than 1 ppmv, thereby further reducing the likelihood of haze formation. Owing to the fact that we consider atmospheres with a low C/O ratio and oxygen levels greater than 10^{-4} PAL, the effects of a haze layer are not considered important (in terms of the Proterozoic Faint Young Sun Paradox) for these reasons.

To summarize, we agree with previous work [21,22,68] after demonstrating that a Proterozoic atmosphere with a negligible CH_4 greenhouse contribution is more likely than one that supports a substantial CH_4 greenhouse. Even present day methane levels appear improbable, and this result is because of our lower O_3 columns (which result in further OH and $\text{O}(^1\text{D})$ production—see the schematic of this in figure 8) which suggest that achieving a methane supported greenhouse during the Mesoproterozoic is even more unlikely than previously estimated. Of course, there are uncertainties in the flux of CH_4 during the Proterozoic, but realistic increases in CH_4 atmospheric flux

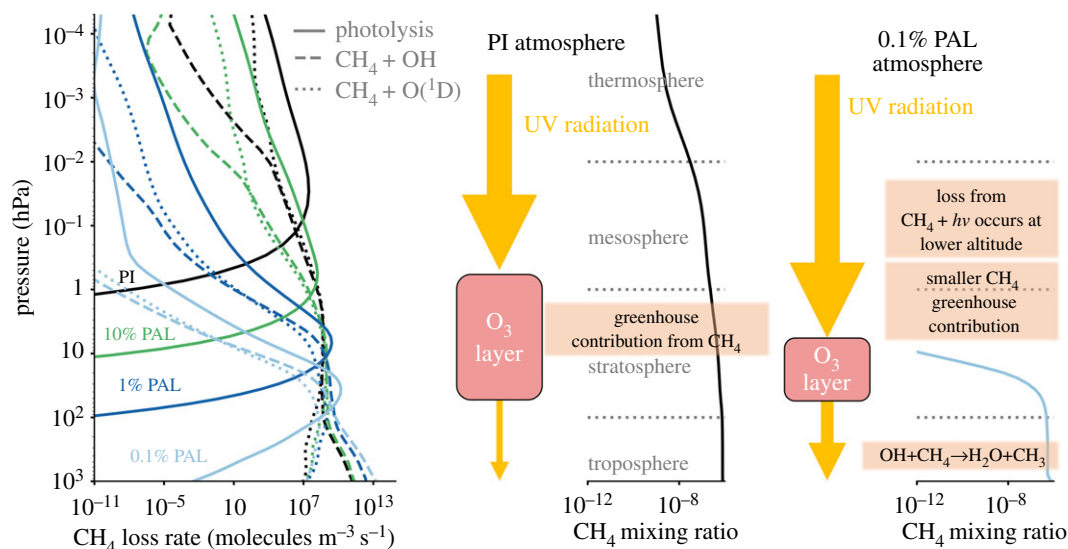


Figure 8. When the O₂ concentration reduces, the mixing ratio of CH₄ reduces. On the left is how the CH₄ loss rate varies with atmospheric pressure for the three major loss mechanisms of CH₄: photolysis, reaction with OH and reaction with O(¹D). Shown alongside the CH₄ mixing ratio profiles for the PI (middle) and 0.1% PAL (right) atmospheres are yellow arrows which indicate UV radiation travelling down through the atmosphere. UV radiation is attenuated by the O₃ layer. When O₂ decreases, the O₃ column abundance decreases, such that increased amounts of UV radiation penetrate into the troposphere. Through photolysis, this produces more OH (e.g. photolysis of H₂O and H₂O₂) and O(¹D) molecules (e.g. photolysis of H₂O, O₂, O₃, and N₂O) which then react with CH₄, decreasing its abundance. CH₄ + hν represents photolysis of CH₄ by a photon with frequency ν, where h is Planck's constant. Note that the size of the arrows and the size of the O₃ layers do not indicate the actual magnitude of relative UV fluxes and O₃ column abundances between atmospheres, respectively.

would not change the atmospheric lifetime of CH₄ enough to mitigate its tropospheric oxidation from OH and O(¹D). Instead of a methane greenhouse, other mechanisms are required to explain a mostly ice-free Proterozoic, such as elevated levels of N₂O (also unlikely due to high rates of photolysis) or CO₂ [63], alterations in the continental coverage [151,152], cloud variability that acts to stabilize the climate system [153], or large-scale mantle thermal mixing variations [154].

Whatever the solution, such low CH₄ mixing ratios have important consequences for predicted exoplanet observations that are based on Early Earth. Additionally, low CH₄ mixing ratios and a cool tropopause from reduced O₃ heating will limit the upward diffusion of hydrogen atoms to the thermosphere, with implications for atmospheric escape and exoplanetary ionospheric observations. These topics will be explored in future work.

5. Conclusion

We used WACCM6, a three-dimensional Earth System Model, to simulate changing oxygen levels since the beginning of the Proterozoic to a pre-industrial atmosphere. Between 0.5% and 50% the present atmospheric level of oxygen, our simulations resulted in significantly lower mean O₃ columns when compared to previous one-dimensional and three-dimensional modelling (figure 6). Based on common literature assumptions, we showed that between 5 and 10 times more O₂ is needed to produce an O₃ layer that fully shields the surface from biologically damaging radiation. As a consequence, we predict that UV surface fluxes were higher than previously estimated for much of Earth's history.

From these new O₃ column predictions, it is likely that the mixing ratio of CH₄ was less than ≈0.1 ppmv for much of the Proterozoic. This is due to a low CH₄ flux to the atmosphere, as well as the increased production of tropospheric OH and O(¹D) from chemical photolysis that we simulate in our model runs. As such, a methane greenhouse is unlikely to solve the Proterozoic Faint Young Sun Paradox.

O₃ is a crucial constituent of Earth's modern atmosphere. These results demonstrate the importance of three-dimensional whole atmosphere chemistry-climate modelling. Better constraints on Proterozoic and Phanerozoic O₂ levels (figure 1) will aid future work in reconstructing the history of Earth's atmosphere, the O₃ layer (based on our new estimates), and linking mass extinction and evolutionary events to the changing O₃ layer.

The O₃ layer varies substantially over a range of O₂ values, and due to its spatial variation, there were likely habitable niches across the globe as O₂ increased and the continents shifted. These fluctuating O₃ column levels through time modulated surface UV fluxes, with consequences for surface life and atmospheric chemistry. Therefore, we recommend that the biological and geological impact of the O₃ layer through time should be re-visited.

Data accessibility. WACCM6 is a publicly available code. The specific release used in this paper was CESM2.1.3, which can be downloaded from the following: https://escomp.github.io/CESM/versions/cesm2.1/html/downloading_cesm.html. Data are available from the Dryad Digital Repository: <https://doi.org/10.5061/dryad.ncjxksvsn> [155].

Authors' contributions. D.R.M., J.-F.L. and B.A.B. initiated the preliminary research. B.A.B. performed preliminary simulations. G.J.C., D.R.M. and J.-F.L. performed the final simulations. G.J.C. produced the figures. All authors analysed and interpreted the simulation output data. G.J.C. wrote the manuscript with input and comments on the final manuscript preparation from all authors.

Competing interests. We declare we have no competing interests.

Funding. G.J.C. acknowledges the studentship funded by the Science and Technology Facilities Council of the United Kingdom (STFC; grant number ST/T506230/1). C.W. acknowledges financial support from the University of Leeds, the Science and Technology Facilities Council, and UK Research and Innovation (grant numbers ST/R000549/1, ST/T000287/1, and MR/T040726/1).

Acknowledgements. We thank an anonymous reviewer, D. S. Abbot, and T. Lyons for their thorough reviews and helpful suggestions which aided in significantly improving the manuscript. Additionally, we thank J. Kasting and other anonymous reviewers for their careful reviews on a previous version of this manuscript. We thank Mark Claire and co-authors [79] for making their solar evolution model publicly available. This work was undertaken on ARC4, part of the High Performance Computing facilities at the University of Leeds, UK. We would like to acknowledge high-performance computing support from Cheyenne (doi:10.5065/D6RX99HX) provided by NCAR's Computational and Information Systems Laboratory, sponsored by the National Science Foundation. The CESM project is supported primarily by the National Science Foundation (NSF). This material is based upon work supported by the National Center for Atmospheric Research (NCAR), which is a major facility sponsored by the NSF under Cooperative Agreement 1852977.

References

- Anbar AD *et al.* 2007 A whiff of oxygen before the Great Oxidation Event? *Science* **317**, 1903–1906. (doi:10.1126/science.1140325)
- Kaufman AJ *et al.* 2007 Late Archean biospheric oxygenation and atmospheric evolution. *Science* **317**, 1900–1903. (doi:10.1126/science.1138700)
- Kendall B, Creaser RA, Reinhard CT, Lyons TW, Anbar AD. 2015 Transient episodes of mild environmental oxygenation and oxidative continental weathering during the late Archean. *Sci. Adv.* **1**, e1500777. (doi:10.1126/sciadv.1500777)
- Catling DC, Zahnle KJ. 2020 The Archean atmosphere. *Sci. Adv.* **6**, eaax1420. (doi:10.1126/sciadv.aax1420)
- Cole DB, Mills DB, Erwin DH, Sperling EA, Porter SM, Reinhard CT, Planavsky NJ. 2020 On the co-evolution of surface oxygen levels and animals. *Geobiology* **18**, 260–281. (doi:10.1111/gbi.12382)
- Dodd MS, Papineau D, Grenne T, Slack JF, Rittner M, Pirajno F, O'Neil J, Little CTS. 2017 Evidence for early life in Earth's oldest hydrothermal vent precipitates. *Nature* **543**, 60–64. (doi:10.1038/nature21377)
- Schopf JW, Kitajima K, Spicuzza MJ, Kudryavtsev AB, Valley JW. 2018 SIMS analyses of the oldest known assemblage of microfossils document their taxon-correlated carbon isotope compositions. *Proc. Natl Acad. Sci. USA* **115**, 53–58. (doi:10.1073/pnas.1718063115)
- Baumgartner RJ, Van Kranendonk MJ, Wacey D, Fiorentini ML, Saunders M, Caruso S, Pages A, Homann M, Guagliardo P. 2019 Nano-porous pyrite and organic matter in 3.5-billion-year-old stromatolites record primordial life. *Geology* **47**, 1039–1043. (doi:10.1130/G46365.1)
- Sánchez-Baracaldo P, Cardona T. 2020 On the origin of oxygenic photosynthesis and cyanobacteria. *New Phytol.* **225**, 1440–1446. (doi:10.1111/nph.16249)
- Han T-M, Runnegar B. 1992 Megascopic eukaryotic algae from the 2.1-billion-year-old Negaunee Iron-Formation, Michigan. *Science* **257**, 232–235. (doi:10.1126/science.1631544)
- Knoll AH, Javaux EJ, Hewitt D, Cohen P. 2006 Eukaryotic organisms in proterozoic oceans. *Phil. Trans. R. Soc. B* **361**, 1023–1038. (doi:10.1098/rstb.2006.1843)
- Betts HC, Puttick MN, Clark JW, Williams TA, Donoghue PCJ, Pisani D. 2018 Integrated genomic and fossil evidence illuminates life's early evolution and eukaryote origin. *Nat. Ecol. Evol.* **2**, 1556–1562. (doi:10.1038/s41559-018-0644-x)
- Retallack GJ, Krull ES, Thackray GD, Parkinson D. 2013 Problematic um-shaped fossils from a Paleoproterozoic (2.2 Ga) paleosol in South Africa. *Precambrian Res.* **235**, 71–87. (doi:10.1016/j.precamres.2013.05.015)
- Bobrovskiy I, Hope JM, Ivantsov A, Nettersheim BJ, Hallmann C, Brocks JJ. 2018 Ancient steroids establish the Ediacaran fossil Dickinsonia as one of the earliest animals. *Science* **361**, 1246–1249. (doi:10.1126/science.aat7228)
- Sperling EA, Robinson JM, Pisani D, Peterson KJ. 2010 Where's the glass? Biomarkers, molecular clocks, and microRNAs suggest a 200-Myr missing Precambrian fossil record of siliceous sponge spicules. *Geobiology* **8**, 24–36. (doi:10.1111/j.1472-4669.2009.00225.x)
- Gregory BS, Claire MW, Rugheimer S. 2021 Photochemical modelling of atmospheric oxygen levels confirms two stable states. *Earth Planet. Sci. Lett.* **561**, 116818. (doi:10.1016/j.epsl.2021.116818)
- Lyons TW, Reinhard CT, Planavsky NJ. 2014 The rise of oxygen in Earth's early ocean and atmosphere. *Nature* **506**, 307–315. (doi:10.1038/nature13068)
- Olson SL, Schwieterman EW, Reinhard CT, Lyons TW. 2018 *Earth: atmospheric evolution of a habitable planet*, p. 189. Berlin, Germany: Springer.
- Lyons TW, Diamond CW, Planavsky NJ, Reinhard CT, Li C. 2021 Oxygenation, life, and the planetary system during Earth's middle history: an overview. *Astrobiology* **21**, 906–923. (doi:10.1089/ast.2020.2418)
- Pavlov AA, Hurtgen MT, Kasting JF, Arthur MA. 2003 Methane-rich proterozoic atmosphere? *Geology* **31**, 87–90. (doi:10.1130/0091-7613(2003)031<0087:MRPA>2.0.CO;2)
- Olson SL, Reinhard CT, Lyons TW. 2016 Limited role for methane in the mid-Proterozoic greenhouse. *Proc. Natl Acad. Sci. USA* **113**, 11 447–11 452. (doi:10.1073/pnas.1608549113)
- Laakso TA, Schrag DP. 2019 Methane in the Precambrian atmosphere. *Earth Planet. Sci. Lett.* **522**, 48–54. (doi:10.1016/j.epsl.2019.06.022)

23. Warke MR, Di Rocco T, Zerkle AL, Lepland A, Prave AR, Martin AP, Ueno Y, Condon DJ, Claire MW. 2020 The Great Oxidation Event preceded a paleoproterozoic 'snowball Earth'. *Proc. Natl Acad. Sci. USA* **117**, 13 314–13 320. (doi:10.1073/pnas.2003090117)
24. Young GM. 2013 Precambrian supercontinents, glaciations, atmospheric oxygenation, metazoan evolution and an impact that may have changed the second half of Earth history. *Geosci. Front.* **4**, 247–261. (doi:10.1016/j.gsf.2012.07.003)
25. Bahcall JN, Pinsonneault MH, Basu S. 2001 Solar models: current epoch and time dependences, neutrinos, and helioseismological properties. *Astrophys. J.* **555**, 990–1012. (doi:10.1086/321493)
26. Poulton SW, Bekker A, Cumming VM, Zerkle AL, Canfield DE, Johnston DT. 2021 A 200-million-year delay in permanent atmospheric oxygenation. *Nature* **592**, 232–236. (doi:10.1038/s41586-021-03393-7)
27. Gumsley AP, Chamberlain KR, Bleeker W, Söderlund U, de Kock MO, Larsson ER, Bekker A. 2017 Timing and tempo of the Great Oxidation Event. *Proc. Natl Acad. Sci. USA* **114**, 1811–1816. (doi:10.1073/pnas.1608824114)
28. Farquhar J, Bao H, Thieme M. 2000 Atmospheric influence of Earth's earliest sulfur cycle. *Science* **289**, 756–759. (doi:10.1126/science.289.5480.756)
29. Bekker A, Holland HD, Wang PL, Rumble D, Stein HJ, Hannah JL, Coetzee LL, Beukes NJ. 2004 Dating the rise of atmospheric oxygen. *Nature* **427**, 117–120. (doi:10.1038/nature02260)
30. Luo G, Ono S, Beukes NJ, Wang DT, Xie S, Summons RE. 2016 Rapid oxygenation of Earths atmosphere 2.33 billion years ago. *Sci. Adv.* **2**, e1600134–e1600134. (doi:10.1126/sciadv.1600134)
31. Bekker A, Holland HD. 2012 Oxygen overshoot and recovery during the early Paleoproterozoic. *Earth Planet. Sci. Lett.* **317**, 295–304. (doi:10.1016/j.epsl.2011.12.012)
32. Canfield DE *et al.* 2013 Oxygen dynamics in the aftermath of the Great Oxidation of Earth's atmosphere. *Proc. Natl Acad. Sci. USA* **110**, 16 736–16 741. (doi:10.1073/pnas.1315570110)
33. Holland HD. 2006 The oxygenation of the atmosphere and oceans. *Phil. Trans. R. Soc. B* **361**, 903–915. (doi:10.1098/rstb.2006.1838)
34. Goldblatt C, Lenton TM, Watson AJ. 2006 Bistability of atmospheric oxygen and the Great Oxidation. *Nature* **443**, 683–686. (doi:10.1038/nature05169)
35. Campbell IH, Squire RJ. 2010 The mountains that triggered the late Neoproterozoic increase in oxygen: the second Great Oxidation Event. *Geochim. Cosmochim. Acta* **74**, 4187–4206. (doi:10.1016/j.gca.2010.04.064)
36. Och LM, Shields-Zhou GA. 2012 The Neoproterozoic oxygenation event: environmental perturbations and biogeochemical cycling. *Earth Sci. Rev.* **110**, 26–57. (doi:10.1016/j.earscirev.2011.09.004)
37. Large RR, Mukherjee I, Gregory D, Steadman J, Corkrey R, Danyushevsky LV. 2019 Atmosphere oxygen cycling through the Proterozoic and Phanerozoic. *Miner. Deposita* **54**, 485–506. (doi:10.1007/s00126-019-00873-9)
38. Kump LR. 2008 The rise of atmospheric oxygen. *Nature* **451**, 277–278. (doi:10.1038/nature06587)
39. Schachat SR, Labandeira CC, Saltzman MR, Cramer BD, Payne JL, Boyce CK. 2018 Phanerozoic pO_2 and the early evolution of terrestrial animals. *Proc. R. Soc. B* **285**, 20172631. (doi:10.1098/rspb.2017.2631)
40. Brand U, Davis AM, Shaver KK, Blamey NJ, Heizler M, Lécuyer C. 2021 Atmospheric oxygen of the paleozoic. *Earth Sci. Rev.* **216**, 103560. (doi:10.1016/j.earscirev.2021.103560)
41. Sperling EA, Wolock CJ, Morgan AS, Gill BC, Kunzmann M, Halverson GP, MacDonald FA, Knoll AH, Johnston DT. 2015 Statistical analysis of iron geochemical data suggests limited late proterozoic oxygenation. *Nature* **523**, 451–454. (doi:10.1038/nature14589)
42. Wallace MW, Hood AvS, Shuster A, Greig A, Planavsky NJ, Reed CP. 2017 Oxygenation history of the Neoproterozoic to early Phanerozoic and the rise of land plants. *Earth Planet. Sci. Lett.* **466**, 12–19. (doi:10.1016/j.epsl.2017.02.046)
43. Narbonne GM. 2005 The Ediacara biota: Neoproterozoic origin of animals and their ecosystems. *Annu. Rev. Earth Planet. Sci.* **33**, 421–442. (doi:10.1146/annurev.earth.33.092203.122519)
44. Zumberge JA, Love GD, Cárdenas P, Sperling EA, Gunasekera S, Rohrssen M, Grosjean E, Grotzinger JP, Summons RE. 2018 Demosponge steroid biomarker 26-methylstigmastane provides evidence for Neoproterozoic animals. *Nat. Ecol. Evol.* **2**, 1709–1714. (doi:10.1038/s41559-018-0676-2)
45. Nettersheim BJ *et al.* 2019 Putative sponge biomarkers in unicellular Rhizaria question an early rise of animals. *Nat. Ecol. Evol.* **3**, 577–581. (doi:10.1038/s41559-019-0806-5)
46. Love GD, Zumberge JA, Cárdenas P, Sperling EA, Rohrssen M, Grosjean E, Grotzinger JP, Summons RE. 2020 Sources of C 30 steroid biomarkers in Neoproterozoic–Cambrian rocks and oils. *Nat. Ecol. Evol.* **4**, 34–36. (doi:10.1038/s41559-019-1048-2)
47. Hallmann C *et al.* 2020 Reply to: sources of C 30 steroid biomarkers in Neoproterozoic–Cambrian rocks and oils. *Nat. Ecol. Evol.* **4**, 37–39. (doi:10.1038/s41559-019-1049-1)
48. Bobrovskiy I, Hope JM, Nettersheim BJ, Volkman JK, Hallmann C, Brocks JJ. 2021 Algal origin of sponge sterane biomarkers negates the oldest evidence for animals in the rock record. *Nat. Ecol. Evol.* **5**, 165–168. (doi:10.1038/s41559-020-01334-7)
49. Erwin DH. 2020 The origin of animal body plans: a view from fossil evidence and the regulatory genome. *Development* **147**, dev182899. (doi:10.1242/dev.182899)
50. Chen X *et al.* 2015 Rise to modern levels of ocean oxygenation coincided with the Cambrian radiation of animals. *Nat. Commun.* **6**, 7142. (doi:10.1038/ncomms8142)
51. Zhang X, Cui L. 2016 Oxygen requirements for the cambrian explosion. *J. Earth Sci.* **27**, 187–195. (doi:10.1007/s12583-016-0690-8)
52. Zhao X, Wang X, Shi X, Tang D, Shi Q. 2018 Stepwise oxygenation of early Cambrian ocean controls early metazoan diversification. *Palaeogeogr. Palaeoclimatol. Palaeoecol.* **504**, 86–103. (doi:10.1016/j.palaeo.2018.05.009)
53. Lenton TM, Boyle RA, Poulton SW, Shields-Zhou GA, Butterfield NJ. 2014 Co-evolution of eukaryotes and ocean oxygenation in the Neoproterozoic era. *Nat. Geosci.* **7**, 257–265. (doi:10.1038/ngeo2108)
54. Mills DB, Ward LM, Jones C, Sweeten B, Forth M, Treusch AH, Canfield DE. 2014 Oxygen requirements of the earliest animals. *Proc. Natl Acad. Sci. USA* **111**, 4168–4172. (doi:10.1073/pnas.1400547111)
55. Mills DB, Canfield DE. 2014 Oxygen and animal evolution: did a rise of atmospheric oxygen 'trigger' the origin of animals? *BioEssays* **36**, 1145–1155. (doi:10.1002/bies.201400101)
56. Levine JS, Hays PB, Walker JCG. 1979 The evolution and variability of atmospheric ozone over geological time. *Icarus* **39**, 295–309. (doi:10.1016/0019-1035(79)90172-6)
57. Kasting JF, Donahue TM. 1980 The evolution of atmospheric ozone. *J. Geophys. Res.: Oceans* **85**, 3255–3263. (doi:10.1029/JC085iC06p03255)
58. Segura A, Krelove K, Kasting JF, Sommerlatt D, Meadows V, Crisp D, Cohen M, Mlawer E. 2003 Ozone concentrations and ultraviolet fluxes on earth-like planets around other stars. *Astrobiology* **3**, 689–708. (doi:10.1089/153110703322736024)
59. Benca JP, Duijntee IAP, Looy CV. 2018 UV-B-induced forest sterility: implications of ozone shield failure in Earth's largest extinction. *Sci. Adv.* **4**, e1700618. (doi:10.1126/sciadv.1700618)
60. Marshall JEA, Lakin J, Troth I, Wallace-Johnson SM. 2020 UV-B radiation was the Devonian–Carboniferous boundary terrestrial extinction kill mechanism. *Sci. Adv.* **6**, eaba0768. (doi:10.1126/sciadv.aba0768)
61. Black BA, Lamarque JF, Shields CA, Elkins-Tanton LT, Kiehl JT. 2014 Acid rain and ozone depletion from pulsed Siberian Traps magmatism. *Geology* **42**, 67–70. (doi:10.1130/G34875.1)
62. Margulis L, Walker JCG, Rambler M. 1976 Reassessment of roles of oxygen and ultraviolet light in Precambrian evolution. *Nature* **264**, 620–624. (doi:10.1038/264620a0)
63. Fiorella RP, Sheldon ND. 2017 Equable end Mesoproterozoic climate in the absence of high CO₂. *Geology* **45**, 231–234. (doi:10.1130/G38682.1)
64. Sagan C, Mullen G. 1972 Earth and Mars: evolution of atmospheres and surface temperatures. *Science* **177**, 52–56. (doi:10.1126/science.177.4043.52)
65. Kasting JF. 2010 Early Earth: faint young Sun redux. *Nature* **464**, 687–689. (doi:10.1038/464687a)
66. Feulner G. 2012 The Faint Young Sun problem. *Rev. Geophys.* **50**, RG2006. (doi:10.1029/2011RG000375)
67. Charnay B, Wolf ET, Marty B, Forget F. 2020 Is the Faint Young Sun problem for Earth solved? *Space Sci. Rev.* **216**, 90. (doi:10.1007/s11214-020-00711-9)
68. Daines SJ, Lenton TM. 2016 The effect of widespread early aerobic marine ecosystems on methane cycling and the Great Oxidation. *Earth Planet. Sci. Lett.* **434**, 42–51. (doi:10.1016/j.epsl.2015.11.021)

69. Kasting JF, Catling D. 2003 Evolution of a habitable planet. *Annu. Rev. Astron. Astrophys.* **41**, 429–463. (doi:10.1146/annurev.astro.41.071601.170049)
70. Gettelman A *et al.* 2019 The whole atmosphere community climate model version 6 (WACCM6). *J. Geophys. Res. (Atmos.)* **124**, 12 380–12 403. (doi:10.1029/2019JD030943)
71. Danabasoglu G *et al.* 2020 The community earth system model version 2 (CESM2). *J. Adv. Model. Earth Syst.* **12**, e01916. (doi:10.1029/2019MS001916)
72. Marsh DR, Mills MJ, Kinnison DE, Lamarque J-F, Calvo N, Polvani LM. 2013 Climate change from 1850 to 2005 simulated in CESM1 (WACCM). *J. Clim.* **26**, 7372–7391. (doi:10.1175/JCLI-D-12-00558.1)
73. Pettit J, Randall CE, Marsh DR, Bardeen CG, Qian L, Jackman CH, Woods TN, Coster A, Harvey VL. 2018 Effects of the September 2005 solar flares and solar proton events on the middle atmosphere in WACCM. *J. Geophys. Res. (Space Phys.)* **123**, 5747–5763. (doi:10.1029/2018JA025294)
74. Proedrou E, Hocke K. 2016 Characterising the three-dimensional ozone distribution of a tidally locked Earth-like planet. *Earth Planets Space* **68**, 96. (doi:10.1186/s40623-016-0461-x)
75. Proedrou E, Hocke K, Wurz P. 2016 The middle atmospheric circulation of a tidally locked Earth-like planet and the role of the sea surface temperature. *Prog. Earth Planet. Sci.* **3**, 22. (doi:10.1186/s40645-016-0098-1)
76. Chen H, Wolf ET, Zhan Z, Horton DE. 2019 Habitability and spectroscopic observability of warm *M*-dwarf exoplanets evaluated with a 3D chemistry-climate model. *Astrophys. J.* **886**, 16. (doi:10.3847/1538-4357/ab4f7e)
77. Chen H, Zhan Z, Youngblood A, Wolf ET, Feinstein AD, Horton DE. 2021 Persistence of flare-driven atmospheric chemistry on rocky habitable zone worlds. *Nat. Astron.* **5**, 298–310. (doi:10.1038/s41550-020-01264-1)
78. Roberson AL, Roadt J, Halevy I, Kasting JF. 2011 Greenhouse warming by nitrous oxide and methane in the Proterozoic Eon. *Geobiology* **9**, 313–320. (doi:10.1111/j.1472-4669.2011.00286.x)
79. Claire MW, Sheets J, Cohen M, Ribas I, Meadows VS, Catling DC. 2012 The evolution of solar flux from 0.1 nm to 160 μm : quantitative estimates for planetary studies. *Astrophys. J.* **757**, 95. (doi:10.1088/0004-637X/757/1/95)
80. Carnall AC. 2017 SpectRes: a fast spectral resampling tool in python. E-prints (<https://arxiv.org/abs/1705.05165>).
81. Tomkins AG, Bowll L, Genge M, Wilson SA, Brand HEA, Wykes JL. 2016 Ancient micrometeorites suggestive of an oxygen-rich Archaean upper atmosphere. *Nature* **533**, 235–238. (doi:10.1038/nature17678)
82. Rimmer PB, Shorttle O, Rugheimer S. 2019 Oxidised micrometeorites as evidence for low atmospheric pressure on the early Earth. *Geochem. Perspect. Lett.* **9**, 38. (doi:10.7185/geochemlet.1903)
83. Payne RC, Brownlee D, Kasting JF. 2020 Oxidized micrometeorites suggest either high $p\text{CO}_2$ or low $p\text{N}_2$ during the Neoproterozoic. *Proc. Natl Acad. Sci. USA* **117**, 1360–1366. (doi:10.1073/pnas.1910698117)
84. Lehmer OR, Catling DC, Buick R, Brownlee DE, Newport S. 2020 Atmospheric CO_2 levels from 2.7 billion years ago inferred from micrometeorite oxidation. *Sci. Adv.* **6**, eaay4644. (doi:10.1126/sciadv.aay4644)
85. Pack A, Höweling A, Hezel DC, Stefanak MT, Beck A-K, Peters STM, Sengupta S, Herwartz D, Folco L. 2017 Tracing the oxygen isotope composition of the upper Earth's atmosphere using cosmic spherules. *Nat. Commun.* **8**, 15702. (doi:10.1038/ncomms15702)
86. Chapman S. 1930 XXXV. On ozone and atomic oxygen in the upper atmosphere. *Lond. Edinb. Dublin Phil. Mag. J. Sci.* **10**, 369–383. (doi:10.1080/14786443009461588)
87. Lary DJ. 1997 Catalytic destruction of stratospheric ozone. *J. Geophys.* **102**, 21 515–21 526. (doi:10.1029/97JD00912)
88. Lee Grenfell J, Lehmann R, Mieth P, Langematz U, Steil B. 2006 Chemical reaction pathways affecting stratospheric and mesospheric ozone. *J. Geophys. Res. (Atmos.)* **111**, D17311. (doi:10.1029/2004JD005713)
89. Emmons LK *et al.* 2020 The chemistry mechanism in the community earth system model version 2 (CESM2). *J. Adv. Model. Earth Syst.* **12**, e01882. (doi:10.1029/2019MS001882)
90. Kinnison DE *et al.* 2007 Sensitivity of chemical tracers to meteorological parameters in the MOZART-3 chemical transport model. *J. Geophys. Res. (Atmos.)* **112**, D20302. (doi:10.1029/2006JD007879)
91. Brasseur GP, Solomon S. 2005 *Aeronomy of the middle atmosphere: chemistry and physics of the stratosphere and mesosphere*. Berlin, Germany: Springer.
92. Butchart N. 2014 The Brewer-Dobson circulation. *Rev. Geophys.* **52**, 157–184. (doi:10.1002/2013RG000448)
93. Cohen NY, Gerber EP, Bühler O. 2014 What drives the Brewer-Dobson circulation? *J. Atmos. Sci.* **71**, 3837–3855. (doi:10.1175/JAS-D-14-0021.1)
94. Way MJ *et al.* 2017 Resolving orbital and climate keys of Earth and extraterrestrial environments with dynamics (ROCKE-3D) 1.0: a general circulation model for simulating the climates of rocky planets. *Astrophys. J. Suppl. Ser.* **231**, 12. (doi:10.3847/1538-4365/aa7a06)
95. Berkner LV, Marshall LC. 1965 On the origin and rise of oxygen concentration in the Earth's atmosphere. *J. Atmos. Sci.* **22**, 225–261. (doi:10.1175/1520-0469(1965)022<0225:OTOARO>2.0.CO;2)
96. Ratner MI, Walker JCG. 1972 Atmospheric ozone and the history of life. *J. Atmos. Sci.* **29**, 803–808. (doi:10.1175/1520-0469(1972)029<0803:AOATHO>2.0.CO;2)
97. Pikuta EV, Hoover RB, Tang J. 2007 Microbial extremophiles at the limits of life. *Crit. Rev. Microbiol.* **33**, 183–209. (doi:10.1080/10408410701451948)
98. Núñez-Pons L, Avila C, Romano G, Verde C, Giordano D. 2018 UV-protective compounds in marine organisms from the Southern ocean. *Mar. Drugs* **16**, 336. (doi:10.3390/md16090336)
99. Gill SS, Anjum NA, Gill R, Jha M, Tuteja N. 2015 DNA damage and repair in plants under ultraviolet and ionizing radiations. *Sci. World J.* **2015**, 250158. (doi:10.1155/2015/250158)
100. Singh SP, Häder D-P, Sinha RP. 2010 Cyanobacteria and ultraviolet radiation (uvr) stress: mitigation strategies. *Ageing Res. Rev.* **9**, 79–90. (doi:10.1016/j.arr.2009.05.004)
101. Sinha RP, Häder D-P. 2002 UV-induced DNA damage and repair: a review. *Photochem. Photobiol. Sci.* **1**, 225–236. (doi:10.1039/B201230H)
102. Rambler MB, Margulis L. 1980 Bacterial resistance to ultraviolet irradiation under anaerobiosis: implications for pre-phanerozoic evolution. *Science* **210**, 638–640. (doi:10.1126/science.7001626)
103. Abreva YA, Leitzinger M, Oppezzo OJ, Odert P, Patel MR, Luna GJM, Forte Giacobone AF, Hansmeier A. 2020 The UV surface habitability of Proxima b: first experiments revealing probable life survival to stellar flares. *Mon. Not. R. Astron. Soc.* **494**, L69–L74. (doi:10.1093/mnras/slaa037)
104. Nawkar GM, Maibam P, Park JH, Sahi VP, Lee SY, Kang CH. 2013 UV-induced cell death in plants. *Int. J. Mol. Sci.* **14**, 1608–1628. (doi:10.3390/ijms14011608)
105. Davies RE, Forbes PD. 1986 Effect of UV radiation on survival of non-haired mice. *Photochem. Photobiol.* **43**, 267–274. (doi:10.1111/j.1751-1097.1986.tb05604.x)
106. Borgeraas J, Hessen DO. 2000 UV-B induced mortality and antioxidant enzyme activities in *Daphnia magna* at different oxygen concentrations and temperatures. *J. Plankton Res.* **22**, 1167–1183. (doi:10.1093/plankt/22.6.1167)
107. Kouwenberg JHM, Broman HI, Cullen JJ, Davis RF, St-Pierre J-F, Runge JA. 1999 Biological weighting of ultraviolet (280–400 nm) induced mortality in marine zooplankton and fish. I. Atlantic cod (*Gadus morhua*) eggs. *Mar. Biol.* **134**, 269–284. (doi:10.1007/s002270050545)
108. Häder D-P, Williamson CE, Wängberg S-Å, Rautio M, Rose KC, Gao K, Helbing EW, Sinha RP, Worrest R. 2015 Effects of UV radiation on aquatic ecosystems and interactions with other environmental factors. *Photochem. Photobiol. Sci.* **14**, 108–126. (doi:10.1039/C4PP90035A)
109. Sagan C. 1973 Ultraviolet selection pressure on the earliest organisms. *J. Theor. Biol.* **39**, 195–200. (doi:10.1016/0022-5193(73)90216-6)
110. Rothschild LJ. 1999 The influence of UV radiation on protistan evolution. *J. Eukaryot. Microbiol.* **46**, 548–555. (doi:10.1111/j.1550-7408.1999.tb06074.x)
111. Cockell CS, Rettberg P, Rabbow E, Olsson-Francis K. 2011 Exposure of phototrophs to 548 days in low earth orbit: microbial selection pressures in outer space and on early earth. *ISME J.* **5**, 1671–1682. (doi:10.1038/ismej.2011.46)
112. Bond DPG, Grasby SE. 2017 On the causes of mass extinctions. *Palaeogeogr. Palaeoclimatol. Palaeoecol.* **478**, 3–29. (doi:10.1016/j.palaeo.2016.11.005)
113. LaViolette PA. 2011 Evidence for a solar flare cause of the pleistocene mass extinction. *Radiocarbon* **53**, 303–323. (doi:10.1017/S003822200056575)

114. Cockell CS, Raven JA. 2007 Ozone and life on the Archaean Earth. *Phil. Trans. R. Soc. A* **365**, 1889–1901. (doi:10.1098/rsta.2007.2049)
115. Cockell CS, Horneck G. 2001 The history of the UV radiation climate of the earth-theoretical and space-based observations. *Photochem. Photobiol.* **73**, 447–451. (doi:10.1562/0031-8655(2001)0730447:THOTUR2.0.CO2)
116. Cockell CS. 1999 Crises and extinction in the fossil record—a role for ultraviolet radiation? *Paleobiology* **25**, 212–225. (doi:10.1017/S0094837300026518)
117. Zedek F, Bureš P. 2018 Holocentric chromosomes: from tolerance to fragmentation to colonization of the land. *Ann. Bot.* **121**, 9–16. (doi:10.1093/aob/mcx118)
118. Zedek F, Veselý P, Tichý L, Elliott TL, Garbolino E, de Ruffray P, Bureš P. 2021 Holocentric plants are more competitive under higher UV-B doses. *New Phytol.* **233**, 15–21. (doi:10.1111/nph.17750)
119. Paul ND, Gwynn-Jones D. 2003 Ecological roles of solar UV radiation: towards an integrated approach. *Trends Ecol. Evol.* **18**, 48–55. (doi:10.1016/S0169-5347(02)00014-9)
120. Bornman JF, Barnes PW, Robson TM, Robinson SA, Jansen MAK, Ballaré CL, Flint SD. 2019 Linkages between stratospheric ozone, uv radiation and climate change and their implications for terrestrial ecosystems. *Photochem. Photobiol. Sci.* **18**, 681–716. (doi:10.1039/C8PP90061B)
121. Tedetti M, Sempéré R. 2006 Penetration of ultraviolet radiation in the marine environment. A review. *Photochem. Photobiol.* **82**, 389–397. (doi:10.1562/2005-11-09-IR-733)
122. Smith RC *et al.* 1992 Ozone depletion: ultraviolet radiation and phytoplankton biology in Antarctic waters. *Science* **255**, 952–959. (doi:10.1126/science.1546292)
123. Llabrés M, Agustí S. 2010 Effects of ultraviolet radiation on growth, cell death and the standing stock of Antarctic phytoplankton. *Aquat. Microb. Ecol.* **59**, 151–160. (doi:10.3354/ame01392)
124. Bancroft BA, Baker NJ, Blaustein AR. 2007 Effects of UVB radiation on marine and freshwater organisms: a synthesis through meta-analysis. *Ecol. Lett.* **10**, 332–345. (doi:10.1111/j.1461-0248.2007.01022.x)
125. Llabrés M, Agustí S, Fernández M, Canepa A, Maurin F, Vidal F, Duarte CM. 2013 Impact of elevated UVB radiation on marine biota: a meta-analysis. *Glob. Ecol. Biogeogr.* **22**, 131–144. (doi:10.1111/j.1466-8238.2012.00784.x)
126. Mloszewska AM, Cole DB, Planavsky NJ, Kappler A, Whitford DS, Ovttrim GW, Konhauser KO. 2018 UV radiation limited the expansion of cyanobacteria in early marine photic environments. *Nat. Commun.* **9**, 3088. (doi:10.1038/s41467-018-05520-x)
127. Kasting JF. 1987 Theoretical constraints on oxygen and carbon dioxide concentrations in the Precambrian atmosphere. *Precambrian Res.* **34**, 205–229. (doi:10.1016/0301-9268(87)90001-5)
128. Madronich S, McKenzie RL, Björn LO, Caldwell MM. 1998 Changes in biologically active ultraviolet radiation reaching the earth's surface. *J. Photochem. Photobiol. B* **46**, 5–19. (doi:10.1016/S1011-1344(98)00182-1)
129. Rugheimer S, Segura A, Kaltenegger L, Sasselov D. 2015 UV surface environment of earth-like planets orbiting FGKM stars through geological evolution. *Astrophys. J.* **806**, 137. (doi:10.1088/0004-637X/806/1/137)
130. Catling DC, Claire MW. 2005 How Earth's atmosphere evolved to an oxic state: a status report. *Earth Planet. Sci. Lett.* **237**, 1–20. (doi:10.1016/j.epsl.2005.06.013)
131. Gebauer S, Grenfell JL, Stock JW, Lehmann R, Godolt M, von Paris P, Rauer H. 2017 Evolution of earth-like extrasolar planetary atmospheres: assessing the atmospheres and biospheres of early earth analog planets with a coupled atmosphere biogeochemical model. *Astrobiology* **17**, 27–54. (doi:10.1089/ast.2015.1384)
132. Crockford PW *et al.* 2018 Triple oxygen isotope evidence for limited mid-Proterozoic primary productivity. *Nature* **559**, 613–616. (doi:10.1038/s41586-018-0349-y)
133. Olson SL, Schwieterman EW, Reinhard CT, Ridgwell A, Kane SR, Meadows VS, Lyons TW. 2018 Atmospheric seasonality as an exoplanet biosignature. *Astrophys. J. Lett.* **858**, L14. (doi:10.3847/2041-8213/aac171)
134. Reinhard CT, Olson SL, Schwieterman EW, Lyons TW. 2017 False negatives for remote life detection on ocean-bearing planets: lessons from the early earth. *Astrobiology* **17**, 287–297. (doi:10.1089/ast.2016.1598)
135. Schwieterman E, Reinhard C, Olson S, Lyons T. 2018 The importance of UV capabilities for identifying inhabited exoplanets with next generation space telescopes. E-prints (<https://arxiv.org/abs/1801.02744>).
136. Stüeken EE, Som SM, Claire M, Rugheimer S, Scherf M, Sproß L, Tosi N, Ueno Y, Lammer H. 2020 Mission to planet Earth: the first two billion years. *Space Sci. Rev.* **216**, 31. (doi:10.1007/s11214-020-00652-3)
137. Reinhard C *et al.* 2019 The remote detectability of Earth's biosphere through time and the importance of UV capability for characterizing habitable exoplanets. *Bull. Am. Astron. Soc.* **51**, 526.
138. Pierazzo E, Garcia RR, Kinnison DE, Marsh DR, Lee-Taylor J, Crutzen PJ. 2010 Ozone perturbation from medium-size asteroid impacts in the ocean. *Earth Planet. Sci. Lett.* **299**, 263–272. (doi:10.1016/j.epsl.2010.08.036)
139. Heays AN, Bosman AD, van Dishoeck EF. 2017 Photodissociation and photoionisation of atoms and molecules of astrophysical interest. *Astron. Astrophys.* **602**, A105. (doi:10.1051/0004-6361/201628742)
140. Lu HC, Chen HK, Chen HF, Cheng BM, Ogilvie JF. 2010 Absorption cross section of molecular oxygen in the transition $E^3 \Sigma_u^- v = 0 - X^3 \Sigma_g^- v = 0$ at 38 K. *Astron. Astrophys.* **520**, A19. (doi:10.1051/0004-6361/201013998)
141. Huestis DL, Berkowitz J. 2010 Critical evaluation of the photoabsorption cross section of CO₂ from 0.125 to 201.6 nm at room temperature. In *Advances in Geosciences*: vol. 25 (ed. A Bhardwaj). London, UK: World Scientific.
142. Ozaki K, Reinhard CT. 2021 The future lifespan of Earth's oxygenated atmosphere. *Nat. Geosci.* **14**, 138–142. (doi:10.1038/s41561-021-00693-5)
143. Kuntz LB, Laakso TA, Schrag DP, Crowe SA. 2015 Modeling the carbon cycle in Lake Matano. *Geobiology* **13**, 454–461. (doi:10.1111/gbi.12141)
144. Cadeau P *et al.* 2020 Carbon isotope evidence for large methane emissions to the proterozoic atmosphere. *Sci. Rep.* **10**, 1–13. (doi:10.1038/s41598-020-75100-x)
145. Fakhraee M, Hancisse O, Canfield DE, Crowe SA, Katsev S. 2019 Proterozoic seawater sulfate scarcity and the evolution of ocean-atmosphere chemistry. *Nat. Geosci.* **12**, 375–380. (doi:10.1038/s41561-019-0351-5)
146. Lambrecht N, Katsev S, Wittkop C, Hall SJ, Sheik CS, Picard A, Fakhraee M, Swanner ED. 2020 Biogeochemical and physical controls on methane fluxes from two ferruginous meromictic lakes. *Geobiology* **18**, 54–69. (doi:10.1111/gbi.12365)
147. Camacho A, Miracle MR, Romero-Viana L, Picazo A, Vicente E. 2017. Lake La Cruz, an iron-rich karstic meromictic lake in Central Spain. In *Ecology of meromictic lakes* (eds RD Gulati, ES Zadereev, AG Degermendzhi), pp. 187–233. Berlin, Germany: Springer. (doi:10.1007/978-3-319-49143-1_8)
148. Trainer MG, Pavlov AA, Dewitt HL, Jimenez JL, McKay CP, Toon OB, Tolbert MA. 2006 Inaugural article: organic haze on Titan and the early Earth. *Proc. Natl Acad. Sci. USA* **103**, 18 035–18 042. (doi:10.1073/pnas.0608561103)
149. Pavlov AA, Brown LL, Kasting JF. 2001 UV shielding of NH₃ and O₂ by organic hazes in the Archean atmosphere. *J. Geophys. Res.: Planets* **106**, 23 267–23 288. (doi:10.1029/2000JE001448)
150. Hörst SM, He C, Ugelow MS, Jelinek AM, Pierrehumbert RT, Tolbert MA. 2018 Exploring the atmosphere of neoproterozoic Earth: the effect of O₂ on haze formation and composition. *Astrophys. J.* **858**, 119. (doi:10.3847/1538-4357/aabd7d)
151. Bradley DC. 2011 Secular trends in the geologic record and the supercontinent cycle. *Earth Sci. Rev.* **108**, 16–33. (doi:10.1016/j.earscirev.2011.05.003)
152. Korenaga J, Planavsky NJ, Evans DAD. 2017 Global water cycle and the coevolution of the Earth's interior and surface environment. *Phil. Trans. R. Soc. A* **375**, 20150393. (doi:10.1098/rsta.2015.0393)
153. Goldblatt C, McDonald VL, McCusker KE. 2021 Earth's long-term climate stabilized by clouds. *Nat. Geosci.* **14**, 143–150. (doi:10.1038/s41561-021-00691-7)
154. Jelinek AM, Lenardic A, Pierrehumbert RT. 2020 Ice, fire, or fizzle: the climate footprint of Earth's supercontinental cycles. *Geochem. Geophys. Geosyst.* **21**, e08464. (doi:10.1029/2019GC008464)
155. Cooke G, Marsh D, Walsh C, Black B, Lamarque J-F. 2021 Varied oxygen simulations with WACCM6 (Proterozoic to pre-industrial atmosphere). Dryad Digital Repository. (doi:10.5061/dryad.ncjskxsvn).